Numerical scheme for the 2D Maxwell-Bloch equations modeling ultrashort pulses

COLIN Thierry*, TORRI Vincent†

April 17, 2005

Abstract

In this paper, we present a numerical method for the Maxwell-Bloch equations which modelize the nonlinear interaction between a laser and a crystal. The propagation of the laser involves different time and length scales during the nonlinear long time interaction with the matter. We avoid the use of a mesh size smaller than the wavelength. We do not use the paraxial approximation but we use the fact that the solution is rapidely oscillating. In the spirit of [6], we propose a discretization of a singular equation based on a profile decomposition. We obtain a method which is asymptotic preserving (that is the paraxial approximation made on the discretization gives the discretization of the nonlinear Schrödinger equation). We perform 2D computations. We numerically investigate the effectiveness of the WKB expansion and show that, under some assumptions, it may not be always valid.

AMS Subject Classification: 81V10, 35Q60, 35L45, 65T50, 34E20

Keywords: Maxwell-Bloch equations, Schrödinger equation, WKB expansion, profiles

1 Introduction

1.1 Physical framework

Ultrashort powerful laser pulses enable the study of more and more complex nonlinear situations in optic, like frequency doubling, nonlinear self focusing or Raman growth. The need of numerical simulations increases and one needs accurate and cheap numerical methods that can be used for a wide class of situations.

A lot of different models exist for describing nonlinear phenomena (see [15] for instance). We present here two of them:

- The macroscopic model: the response of the matter to the electro-magnetic wave is measured on a large scale, compared to the wavelength of the laser. In

*MAB, Université de Bordeaux 1, CNRS UMR 5466, 351, cours de la Libération, 33405 Talence cédex. E-mail: colin@math.u-bordeaux.fr

†IECN, CNRS UMR 7502 and Université Henri Poincaré de Nancy 1, B.P. 239, 54506 Vandoeuvre-lès-Nancy Cedex, France. E-mail: torri@iecn.u-nancy.fr

a dimensionless form, one can write such a system (Maxwell-Lorentz system) under the form:

$$\left\{\begin{array}{rcl} \partial_t \mathbf{B} &=& -\mathrm{rot}\,(\mathbf{E})\,, \\ \partial_t \mathbf{E} &=& \mathrm{rot}\,(\mathbf{B}) - \partial_t \mathbf{P}, \\ -\frac{1}{\omega^2}\partial_t^2 \mathbf{P} + \mathbf{P} - \phi \mathbf{P}^3 &=& \chi_1 \mathbf{E}. \end{array}\right.$$

The parameters ω, ϕ and χ_1 are non dimensional parameters and $\mathbf{P}$ is the polarization.

- The semi-classical model: the response of the matter to the electro-magnetic field is given by a quantum dynamic type description (the polarization), whereas the electro-magnetic field is classically given by the Maxwell equations. Such a system (Maxwell-Bloch system) is given by:

$$\left\{\begin{array}{rcl} \partial_t \mathbf{B} &=& -\mathrm{rot}\,(\mathbf{E})\,, \\ \partial_t \mathbf{E} &=& \mathrm{rot}\,(\mathbf{B}) - \partial_t \mathbf{P}, \\ \mathbf{P} &=& n_a \mathrm{Tr}(\rho \mathbf{p}), \end{array}\right.$$

where $\mathbf{p}$ is the dipolar matrix of the atom, ρ is the density matrix (which describes the states of the electron of an atom). The matrix ρ satisfies the optical Bloch equations (see below).

A presentation of these models is given in [9], [4] or [15]. The different scales that occure are the following:

- The wavelength of the laser is about the micrometer and the length of the pulse is between a hundred micrometer and one meter.
- The propagation length is of the millimeter in crystals and of hundred of meter in gas.
- The duration of the pulse stands between 100 femtoseconds (1E-13s) and 10 nanoseconds (1E-8s). The delay of the propagation is about 1E-11s for crystals and about 1E-6s for gas.

Classically, the Maxwell equations are solved by using a finite difference scheme (the Yee scheme for example) and a Cranck-Nicholson method is used for the polarization equation (see [3, 16] for both macroscopic and semi-classic models). The Yee scheme keeps the properties of the continuous operators. But there is a large difference of scales between the wavelength of the signal and its propagation length (the latter being large compared to the former). Hence, using a finite difference method like the Yee scheme leads to a very thin mesh, hence to a huge quantity of data to compute.

1.2 Description of the method

The aim of this paper is to extend the method of [6] in a 2-D context, using a pseudo-spectral method and to get rid of the moving window technic. We study the semi-classical model (the Maxwell-Bloch equations), when the matter is a crystal composed of atoms whose electrons have 2 levels of energy. The signal will propagate on long time.

As mentioned in the previous paragraph, we deal with a signal involving different scales. More precisely, for dimensionless variables, the oscillatory frequency of the signal is of order $\frac{1}{\varepsilon}$ ($\varepsilon \ll 1$), and the signal propagates on large distances (typically of order $\frac{1}{\varepsilon}$). This implies that a finite difference scheme must have a number of discretization points (in the space domain) of order $\frac{N_x}{\varepsilon}$ ($N_x \gg 1$) and a number of discretization points in the time domain of order $\frac{N_t}{\varepsilon^2}$, ($N_t \gg 1$).

We want to get rid of these different scales, so that the time-space domain will be discretized with $N_x \times N_t$ points, that is a gain of ε^{-3} points. More precisely, we will see in section 3 that the Maxwell-Bloch equations enter the following class of systems:

$$\partial_t V^\varepsilon(t,\mathbf{x}) + A(\partial_\mathbf{x})V^\varepsilon(t,\mathbf{x}) + \frac{L_0}{\varepsilon}V^\varepsilon(t,\mathbf{x}) = F(V^\varepsilon(t,\mathbf{x})), \tag{1}$$

where $t \in \mathbb{R}$, $\mathbf{x} = (x_1, \cdots, x_d) \in \mathbb{R}^d$, $A(\partial_\mathbf{x}) = \sum_{i=1}^d A_i \partial_{x_i}$, A_i being symmetric matrices, L_0 being a skew-symmetric one, $F : \mathbb{R}^p \to \mathbb{R}^p$ is a smooth mapping and ε the small parameter. The initial datum is given by

$$V^\varepsilon(0,\mathbf{x}) = e^{\frac{i\mathbf{k}.\mathbf{x}}{\varepsilon}} V_0(\mathbf{x}) + c.c.,$$

where *c.c.* denotes the complex conjugate and $\mathbf{k} \in \mathbb{R}^d$ is the wave vector. Those systems has been extensively studied by J.L. Joly, G. Métivier and J. Rauch (see [11], [12] [13]), by Donnat ([9]) and D. Lannes ([14]). Note that the initial data for V^ε is not bounded in any H^s for $s > 0$. It is also the case for the solution to (1). In order to have better properties, the idea is to write V^ε using a profile decomposition $V^\varepsilon(t,\mathbf{x}) = \mathcal{V}^\varepsilon(t,\mathbf{x},\theta)$, where $\theta = \frac{\mathbf{k}.\mathbf{x}-\omega t}{\varepsilon}$ and $(\omega,\mathbf{k}) \in \mathbb{R} \times \mathbb{R}^d$ satisfies the dispersion relation of the medium. We choose a profile which corresponds to what we want to study (long time propagation, small nonlinearity). The phase is modeled by θ (fast variable) and $\mathcal{V}^\varepsilon$ is taken as being periodic with respect to θ.

In our case, as the interaction between laser and matter occurs in long time (diffractive optic), we will choose the following profile:

$$V^\varepsilon(t,\mathbf{x}) = \mathcal{V}^\varepsilon\left(\varepsilon t, \mathbf{x} - \nabla_\mathbf{k}\omega t, \frac{\mathbf{k}.\mathbf{x} - \omega t}{\varepsilon}\right), \tag{2}$$

where $\mathbf{x} \in \mathbb{R}^d$ and $\nabla_\mathbf{k}\omega$ being the group velocity.

Of course, the profile $\mathcal{V}^\varepsilon$ is not well-defined by (2). In order to have a correct definition, we will give the system of equations satisfied by $\mathcal{V}^\varepsilon$. Indeed, if such a profile $\mathcal{V}^\varepsilon(\tau, X, \theta)$ exists, then it satisfies

$$\left(\varepsilon\partial_\tau - \nabla_\mathbf{k}\omega\partial_X - \frac{\omega}{\varepsilon}\partial_\theta\right)\mathcal{V}^\varepsilon + \frac{1}{\varepsilon}\left(A\left(\mathbf{k}\partial_\theta + \varepsilon\partial_X\right) + L_0\right)\mathcal{V}^\varepsilon = \varepsilon F\left(\mathcal{V}^\varepsilon\right), \tag{3}$$

for every $\tau = \varepsilon t$, $X = \mathbf{x} - \nabla_\mathbf{k}\omega t$ and $\theta = \frac{\mathbf{k}.\mathbf{x}-\omega t}{\varepsilon}$. In order to define $\mathcal{V}^\varepsilon$, we impose that it satisfies (3) for $(\tau, X, \theta) \in [0,T] \times \mathbb{R}^d \times [0, 2\pi]$. The initial datum is $\mathcal{V}^\varepsilon(\tau, X, \theta) = e^{i\theta}V_0(\mathbf{x}) + c.c.$.

It is easy to show that there exist solutions to (3), defined on $(\tau, X, \theta) \in [0,T] \times \mathbb{R}^d \times [0, 2\pi]$ that are bounded in $\mathrm{L}^\infty_\tau\left([0,T]; \mathrm{H}^s\left(R^d \times [0, 2\pi]\right)\right)$ with respect to ε, for s large enough. As noticed above, the solution to (1) is not bounded as $\varepsilon \to 0$ whereas that of (3) is. One can therefore suspect that the solution to (3) will be easier to compute than the one of (2). Indeed, V^ε involves oscillations in time and space of

size ε and is defined on a time scale of size $O\left(\frac{1}{\varepsilon}\right)$, while the variation of $\mathcal{V}^\varepsilon$ are of order $O(1)$ and $\tau \mapsto \mathcal{V}^\varepsilon(\tau)$ is defined on a time interval of size $O(1)$.

The main problem is the variable θ. As done in [6], we expand $\mathcal{V}^\varepsilon$ in a Fourier serie with respect to θ. Writing $\mathcal{V}^\varepsilon = \sum_{j\in\mathbb{Z}} \mathcal{V}^\varepsilon{}_j e^{ij\theta}$, we obtain an infinite system of PDE's. Denoting by P_j the projector on the j$^{\text{th}}$ Fourier mode, that is, if $U = \sum_{j\in\mathbb{Z}} U_j e^{ij\theta}$, $P_j(U) = U_j$, one gets

$$\left(\left(\varepsilon\partial_\tau - \nabla_{\mathbf{k}}\omega\partial_X - \frac{ij\omega}{\varepsilon}\right) + \frac{1}{\varepsilon}\left(A\left(ij\mathbf{k} + \varepsilon\partial_X\right) + L_0\right)\right)\mathcal{V}^\varepsilon = \varepsilon P_j\left(F\left(\mathcal{V}^\varepsilon\right)\right),$$

for $j \in \mathbb{Z}$.

As in [6], we truncate this system and in practice, we only need to compute the solution of this equation for $j = 1$ and $j = 3$. Note that the use of the group velocity $\nabla_{\mathbf{k}}\omega$ enables us to get rid of the moving window technics used in 1-D in [6] and allows us to use a pseudo-spectral method for the space discretization.

Classical results (see [9] for instance) show that if $V^\varepsilon(0,\mathbf{x})$ is small enough, then the profile $\mathcal{V}^\varepsilon$ tends to a solution of a nonlinear Schrödinger equation, as ε tends to 0. This result, that we recall below, will be used in order to validate our approach.

1.3 Outline of the paper

This paper is organized as follows:

- In section 2, we recall some results about the obtaining of the Maxwell-Bloch equations. Then we will give a dimensionless form of the equations and the different assumptions that we will make.
- Section 3 will be devoted to the WKB expansion mentioned above. We present the theoretical framework and some known convergence results that we will use later. We will compute explicitly the WKB expansion performed on the Maxwell-Bloch equations. This one will be useful in order to validate our numerical scheme: we will compare our numerical solution with the one given by the asymptotic expansion.
- Section 4 will present the numerical schemes: as we want to validate our numerical results by using the nonlinear Schrödinger equation mentioned above, we briefly present a classical scheme to compute it. Then the numerical scheme of the Maxwell-Bloch equations will be introduced.
- Finally, section 5 will present the numerical results and their consequences as for the relative behavior of the solution of the Maxwell-Bloch equations and the nonlinear Schrödinger one.

2 Modelization

The aim of this work is to introduce an efficient numerical scheme of the semi-classical model describing the laser-matter interaction. We suppose that the matter is composed of atoms with two-levels energy electrons. First, we briefly recall how the Bloch equations (which describe the response of the matter to the electromagnetic field) are obtained in that case and how they are coupled to the Maxwell

equations. Then, we will put the equations in a dimensionless form and we will set the assumptions that we will make.

2.1 Polarization, optical Bloch equations

For more details about these models, one can see [7], [1] and [4].

Modeling the interaction between a material and an electro-magnetic field consists of coupling the macroscopic quantity $\mathbf{E}$ (the electric field) and $\mathbf{B}$ (the magnetic induction) with the quantum quantity $\mathbf{P}$ (the polarization):

$$\left\{\begin{array}{rcl} \partial_t \mathbf{B} &=& -\mathrm{rot}\,(\mathbf{E}), \\ \varepsilon_0 \partial_t \mathbf{E} &=& \frac{1}{\mu_0}\mathrm{rot}\,(\mathbf{B}) - \partial_t \mathbf{P}, \\ \mathrm{div}\,(\mathbf{B}) &=& 0, \\ \mathrm{div}\,(\mathbf{E}+\mathbf{P}) &=& 0. \end{array}\right. \tag{4}$$

The permittivity ε_0 and the susceptibility μ_0 are those of vacuum. There is no electric density of charges and no electric current, so that the divergences are free. In general, if the density of the atoms by unit of volume of a material is n_a and if the polarization of one atom submitted to an electric field is $\mathbf{P_a}$, then, the polarization $\mathbf{P}$ is equal to $n_a\mathbf{P_a}$. It suffices to compute $\mathbf{P_a}$ with the help of the quantum physics and to find what kind of equations it satisfies.

Let us consider the Hamiltonian H of an atom submitted to an electro-magnetic field $\mathbf{E}$. It can be rewritten as the sum of the non perturbed Hamiltonian H_0 and the perturbed Hamiltonian H_1. In our case (a two-levels energy electron), H_0 is a 2×2 symmetric matrix whose eigenvalues are 0 and $\omega_{1,2}$. The eigenvalue $\omega_{1,2}$ is linked to the energy that the electron must receive to reach the excited state from its stable state of energy. The value of H_1 is $H_1 = -e\,(\mathbf{E},\mathbf{R})\,\mathrm{I_d}$, where e is the charge of an electron, and $\mathbf{R}$ the vector from the center of the atom to the point we are looking at. Finally,

$$\mathbf{P_a} = e\int \mathbf{R}\psi\bar{\psi}\mathrm{d}\Omega, \tag{5}$$

where ψ is a state of the electron.

To obtain the equation satisfied by $\mathbf{P_a}$, we introduce a_1 and a_2, the projections of a state ψ respectively on ψ_1 and ψ_2, the two eigenvectors of H_0 respectively associated to the eigenvalues 0 and $\omega_{1,2}$. From (5), it is easy to show that

$$\mathbf{P_a} = 2\mathrm{Re}\,(a_1\overline{a_2}\mathbf{p_{1,2}}),$$

where $\mathbf{p_{1,2}}$ is a fixed vector which depends only on the atom (it is the polarization vector of the atom).

From the Schrödinger equation

$$i\hbar\frac{\mathrm{d}\psi}{\mathrm{d}t} = H\psi, \tag{6}$$

we deduce the optical Bloch equations satisfied by a_1 and a_2:

$$\partial_t\begin{pmatrix} a_1 \\ a_2 \end{pmatrix} = i\begin{pmatrix} 0 & \frac{(\mathbf{E},\mathbf{p_{1,2}})}{\hbar} \\ \frac{(\mathbf{E},\mathbf{p_{1,2}})}{\hbar} & -\omega_{1,2} \end{pmatrix}\begin{pmatrix} a_1 \\ a_2 \end{pmatrix}. \tag{7}$$

Finally, the Maxwell-Bloch equations are

$$\left\{\begin{array}{rcl} \partial_t \mathbf{B} &=& -\mathrm{rot}\,(\mathbf{E}) \\ \varepsilon_0 \partial_t \mathbf{E} &=& \frac{1}{\mu_0}\mathrm{rot}\,(\mathbf{B}) - \partial_t \mathbf{P} \\ \mathbf{P} &=& 2n_a \mathrm{Re}\,(a_1\overline{a_2}\mathbf{p_{1,2}}) \\ \partial_t \begin{pmatrix} a_1 \\ a_2 \end{pmatrix} &=& i \begin{pmatrix} 0 & \frac{(\mathbf{E},\mathbf{p_{1,2}})}{\hbar} \\ \frac{(\mathbf{E},\mathbf{p_{1,2}})}{\hbar} & -\omega_{1,2} \end{pmatrix} \begin{pmatrix} a_1 \\ a_2 \end{pmatrix}. \end{array}\right. \tag{8}$$

Remark 2.1 *The quantity $|a_i|^2$ is the probability that the electron is in the state i ($i = 1, 2$). It follows that $|a_1|^2 + |a_2|^2 = 1$.*

We now give a dimensionless form of (8).

2.2 Dimensionless form of the equations

We introduce $\mathbf{R} = a_1\overline{a_2}\mathbf{p_{1,2}}$, the complex polarization and $N = 1 - |a_1|^2 + |a_2|^2$. The Bloch equation (7) allows us to write

$$\partial_t \mathbf{R} = i\omega_{1,2}\mathbf{R} + i\frac{(\mathbf{E}, \mathbf{p_{1,2}})}{\hbar}(N-1)\,\mathbf{p_{1,2}}.$$

In order to close the system, we find the equation satisfied by N:

$$\partial_t N = 4\mathrm{Re}\left(i\frac{(\mathbf{E},\mathbf{R})}{\hbar}\right) = -4\mathrm{Im}\left(\frac{(\mathbf{E},\mathbf{R})}{\hbar}\right).$$

Recall that $\mathbf{E}$ and $\mathbf{p_{1,2}}$ are real vectors. If we note $\mathbf{P}$ and $\mathbf{Q}$ respectively the real part and the imaginary part of $\mathbf{R}$, and p the norm of $\mathbf{p_{1,2}}$, then (8) can be rewritten as

$$\left\{\begin{array}{rcl} \partial_t \mathbf{B} &=& -\mathrm{rot}\,(\mathbf{E}), \\ \partial_t \mathbf{E} &=& \mathrm{rot}\,(\mathbf{B}) + \frac{2n_a\omega_{1,2}}{\varepsilon_0}\mathbf{Q}, \\ \partial_t \mathbf{P} &=& -\omega_{1,2}\mathbf{Q}, \\ \partial_t \mathbf{Q} &=& \omega_{1,2}\mathbf{P} + \frac{N-1}{\hbar}p^2\mathbf{E}, \\ \partial_t N &=& -4\frac{(\mathbf{E},\mathbf{Q})}{\hbar}. \end{array}\right. \tag{9}$$

We introduce the dimensionless variables as follows: the fields E, B, P and Q are given by $E = E_0\tilde{E}$, $B = B_0\tilde{B}$, $P = P_0\tilde{P}$ and $Q = Q_0\tilde{Q}$, where E_0, B_0, P_0 and Q_0 are the reference values which will be fixed later on. The space variables (x, y, z) are given by $(x, y, z) = d(\tilde{x}, \tilde{y}, \tilde{z})$, where d is the length of the pulse. The time t is given by $t = t_0\tilde{t}$, where t_0 is the duration of the pulse.

The velocity of the wave is given by $c = (\varepsilon_0\mu_0)^{-2}$ and the different orders of magnitude are given by:

$$\begin{array}{rcl} t_0 c &=& d, \\ dB_0 &=& t_0 E_0, \\ P_0 &=& Q_0, \\ 2n_a Q_0 &=& \varepsilon_0\sqrt{\alpha}E_0, \end{array}$$

where $\alpha = \frac{2n_a p^2}{\hbar\varepsilon_0\omega_{1,2}}$. The small parameter ε is equal to $\varepsilon = (\omega_{1,2}t_0)^{-1}$. Denoting by

$\beta = 2\left(\frac{E_0 p t_0}{\hbar}\right)^2 \frac{1}{\sqrt{\alpha}}$, the equations become (omitting the tilde notation):

$$\left\{\begin{array}{rcl} \partial_t \mathbf{B} &=& -\mathrm{rot}\,(\mathbf{E})\,, \\ \partial_t \mathbf{E} &=& \mathrm{rot}\,(\mathbf{B}) + \frac{\sqrt{\alpha}}{\varepsilon}\mathbf{Q}, \\ \partial_t \mathbf{P} &=& -\frac{1}{\varepsilon}\mathbf{Q}, \\ \partial_t \mathbf{Q} &=& \frac{1}{\varepsilon}\mathbf{P} + \frac{(N-1)\sqrt{\alpha}}{\varepsilon}\mathbf{E}, \\ \partial_t N &=& -\frac{2\beta}{\varepsilon}\,(\mathbf{E}, \mathbf{Q})\,. \end{array}\right. \tag{10}$$

The physical framework being the one of a high energy laser with short pulse crossing a crystal, the order of magnitude of the physical quantities are (in S.I. units)

Avogadro's number	n_a	1E28
Polarization	p	$1\mathrm{E}-29$
Planck's constant	$\hbar$	$1\mathrm{E}-34$
Permittivity of vacuum	ε_0	$1\mathrm{E}-11$
Self-pulsation of the atom	ω_{12}	1E15
Pulse of the laser	t_0	$1\mathrm{E}-13$
Amplitude of $\mathbf{E}$	E_0	1E8

so that one obtains the following order of magnitude for the parameters:

ε	$1\mathrm{E}-2$
α	1
β	1

Of course, we can simulate less powerful laser (smaller E_0, which gives a smaller ε).

Simplifications: The last equation of (10) has a nonlinear term with large coefficient, which can raise huge numerical problems. Hence, we use the fact that the excited state of the atom is far less populated than the stable one:

$$|a_2| \ll |a_1|\,. \tag{11}$$

As $|a_1|^2 + |a_2|^2 = 1$, one gets

$$N = 1 - \left(1 - |a_2|^2\right) + |a_2|^2 = 2\,|a_2|^2\,. \tag{12}$$

From this equality, we can easily deduce that

$$|\mathbf{R}|^2 = |a_1|^2\,|a_2|^2\,p^2 = \left(1 - |a_2|^2\right)|a_2|^2\,p^2 = \left(1 - \frac{N}{2}\right)\frac{N}{2}p^2, \tag{13}$$

so that N is the root of a polynomial of degree 2. From (12) and (13), we find that

$$N \simeq \frac{2\,|\mathbf{R}|^2}{p^2}. \tag{14}$$

Remark 2.2 *With the dimensionless quantities, one gets*

$$N \simeq \frac{\beta\varepsilon^2}{\sqrt{\alpha}}\left(|\mathbf{P}|^2 + |\mathbf{Q}|^2\right). \tag{15}$$

Note that this approximation can be seen as a particular version of the change of variables introduced in [5] or in [11] that corresponds to some transparency property of the system.

With this approximation, we can get rid off the last equation of (10) so that

$$\left\{\begin{array}{rcl} \partial_t \mathbf{B} &=& -\mathrm{rot}\,(\mathbf{E})\,, \\ \partial_t \mathbf{E} &=& \mathrm{rot}\,(\mathbf{B}) + \frac{\sqrt{\alpha}}{\varepsilon}\mathbf{Q}, \\ \partial_t \mathbf{P} &=& -\frac{1}{\varepsilon}\mathbf{Q}, \\ \partial_t \mathbf{Q} &=& \frac{1}{\varepsilon}\mathbf{P} - \frac{\sqrt{\alpha}}{\varepsilon}\mathbf{E} + \beta\varepsilon\mathbf{E}\left(|\mathbf{P}|^2 + |\mathbf{Q}|^2\right). \end{array}\right. \tag{16}$$

Finally, we restrict ourself to the magnetic transverse mode (the quantities do not depend on the z variable, so that $\mathbf{B}$ has two components b_x and b_y, and $\mathbf{E}$, $\mathbf{P}$ and $\mathbf{Q}$ have one, which are respectively denoted by e, p and q). Hence we obtain the final form of the system that we will study throughout this paper:

$$\left\{\begin{array}{rcl} \partial_t b_x &=& -\partial_y e, \\ \partial_t b_y &=& \partial_x e, \\ \partial_t e &=& \partial_x b_y - \partial_y b_x + \frac{\sqrt{\alpha}}{\varepsilon}q, \\ \partial_t p &=& -\frac{1}{\varepsilon}q, \\ \partial_t q &=& \frac{1}{\varepsilon}p - \frac{\sqrt{\alpha}}{\varepsilon}e + \beta\varepsilon e\left(|p|^2 + |q|^2\right). \end{array}\right. \tag{17}$$

3 WKB expansion

As it has been mentioned in the introduction, we want to compute efficiently a signal which oscillates at the scale ε^{-1} on the time-space domain, and which propagates on a long time (of order ε^{-1}). To achieve this, we will describe the fields thanks to profiles in order to decouple these scales. First, we recall some results about WKB-type expansions, then we will compute the formal WKB expansion of (17) with respect to ε.

3.1 Some tools of diffractive optics

We consider the following class of system:

$$\partial_t V^\varepsilon + A\left(\partial_{\mathbf{x}}\right) V^\varepsilon + \frac{1}{\varepsilon} L_0 V^\varepsilon + \varepsilon F\left(V^\varepsilon\right) = 0, \tag{18}$$

where $t \in [0,T]$, $\mathbf{x} \in \mathbb{R}^n$, $V^\varepsilon : [0,T] \times \mathbb{R}^n \to \mathbb{R}^p$. The operator $A\left(\partial_{\mathbf{x}}\right)$ is defined by $A\left(\partial_{\mathbf{x}}\right) = \sum_{j=1}^n A_j \partial_{x_j}$, where A_j are symetric matrices. The matrix L_0 is skew-symetric and $F : \mathbb{R}^p \to \mathbb{R}^p$ is a smooth map. We give an initial data for (18) which is an oscillatory function:

$$V^\varepsilon(t=0,\mathbf{x}) = V_0(\mathbf{x}) e^{i\frac{\mathbf{k}\mathbf{x}}{\varepsilon}} + c.c.,$$

where *c.c.* denotes the conjugate complex number. The system (17) enters the class of systems (18).

Systems of the form (18) have been studied by J.L. Joly, G. Métivier and J. Rauch (*cf* [11], [12], [13], for example). Applications to nonlinear optics can be found in [9], [10] or [14].

Following [11], we construct solutions of (18) thanks to profiles. We need some notations.

First, we introduce the characteristic variety of the operator $L^\varepsilon(\partial_t, \partial_{\mathbf{x}}) = \partial_t + A(\partial_{\mathbf{x}}) + \frac{1}{\varepsilon}L_0$. For $\mathbf{k} = (k_1, \cdots, k_n) \in \mathbb{R}^n$ and $\omega \in \mathbb{R}$, we denote by $L(\omega, \mathbf{k}) = -i\omega + i\sum_{j=1}^n k_j A_j + L_0$ and the characteristic variety is defined by

$$\mathrm{Char}(L^\varepsilon) = \{(\omega, \mathbf{k}) \in \mathbb{R} \times \mathbb{R}^n \ s.t. \ \det(L(\omega, \mathbf{k})) = 0\}.$$

The relation $\det(L(\omega, \mathbf{k})) = \det\left(-i\omega + i\sum_{j=1}^n k_j A_j + L_0\right) = 0$ is called the dispersion relation. The set $\mathrm{Char}(L^\varepsilon)$ is an algebraic variety. At a regular point of $\mathrm{Char}(L^\varepsilon)$, one can differentiate the function $\mathbf{k} \mapsto \omega(\mathbf{k})$ and its gradient $\nabla_{\mathbf{k}}\omega$ is called the group velocity.

The solution V^ε of (18) is then described by a profile $\mathcal{V}^\varepsilon(\tau, \mathbf{X}, \theta)$ as follows:

$$V^\varepsilon(t, \mathbf{x}) = \mathcal{V}^\varepsilon\left(\varepsilon t, \mathbf{x} - \nabla_{\mathbf{k}}\omega t, \frac{(\mathbf{k}, \mathbf{x}) - \omega t}{\varepsilon}\right). \tag{19}$$

$\mathcal{V}^\varepsilon$ is supposed to be periodic with respect to θ.

Of course, (19) does not define $\mathcal{V}^\varepsilon$. If we inject $\mathcal{V}^\varepsilon$ in (18), one gets:

$$\left(\varepsilon\partial_\tau - \nabla_{\mathbf{k}}\omega.\nabla_{\mathbf{X}} - \frac{\omega}{\varepsilon}\partial_\theta\right)\mathcal{V}^\varepsilon(\tau, \mathbf{X}, \theta) + A\left(\partial_{\mathbf{X}} + \frac{\mathbf{k}}{\varepsilon}\partial_\theta\right)\mathcal{V}^\varepsilon(\tau, \mathbf{X}, \theta) + \frac{1}{\varepsilon}L_0\mathcal{V}^\varepsilon(\tau, \mathbf{X}, \theta) = \varepsilon F(\mathcal{V}^\varepsilon(\tau, \mathbf{X}, \theta)), \tag{20}$$

for all $\tau = \varepsilon t$, $\mathbf{X} = \mathbf{x} - \nabla_{\mathbf{k}}\omega t$ and $\theta = \frac{\mathbf{k}.\mathbf{x} - \omega t}{\varepsilon}$.

In order to define precisely $\mathcal{V}^\varepsilon$, we actually impose that (20) is satisfied for all τ, $\mathbf{X}$ and θ. Hence we obtain the singular equation, which is given by:

$$\left(\varepsilon\partial_\tau - \nabla_{\mathbf{k}}\omega.\nabla_{\mathbf{X}} - \frac{\omega}{\varepsilon}\partial_\theta\right)\mathcal{V}^\varepsilon(\tau, \mathbf{X}, \theta) + \frac{1}{\varepsilon}\left(A(\varepsilon\partial_{\mathbf{X}} + \mathbf{k}\partial_\theta) + L_0\right)\mathcal{V}^\varepsilon(\tau, \mathbf{X}, \theta) = \varepsilon F(\mathcal{V}^\varepsilon(\tau, \mathbf{X}, \theta)), \tag{21}$$

for all $\tau \in [0, T]$, $\mathbf{X} \in \mathbb{R}^n$ and $\theta \in [0, 2\pi]$, the initial datum being

$$\mathcal{V}^\varepsilon(0, \mathbf{X}, \theta) = \left(e^{i\theta}V_0(\mathbf{x}) + c.c.\right).$$

The following proposition is obvious:

Proposition 3.1 *If $\mathcal{V}^\varepsilon$ is a solution of (21) on $(\tau, \mathbf{X}, \theta) \in [0, T] \times \mathbb{R}^n \times [0, 2\pi]$, then $V^\varepsilon(t, \mathbf{x}) = \mathcal{V}^\varepsilon\left(\varepsilon t, \mathbf{x} - \nabla_{\mathbf{k}}\omega t, \frac{\mathbf{k}.\mathbf{x} - \omega t}{\varepsilon}\right)$ is a solution of (19) on $(t, \mathbf{x}) \in [0, \frac{T}{\varepsilon}] \times \mathbb{R}^n$.*

Remark 3.1 *The systematic use of equation (21) instead of (18) allows to work on functions $\mathcal{V}^\varepsilon(\tau, \mathbf{X}, \theta)$ which are in Sobolev spaces $\mathrm{H}^s_{\mathbf{X},\theta}(\mathbb{R}^n \times [0, 2\pi])$ and are bounded with respect to ε, which is not the case for V^ε, whose initial data $e^{\frac{i\mathbf{k}.\mathbf{x}}{\varepsilon}}V_0(\mathbf{x}) + cc$ is not bounded independantly of ε.*

Remark 3.2 *General theorems give the existence of solutions of (21) on correct time interval. In this paper, we will show how to use the singular equation (21) for numerical purpose. One has for example:*

Theorem 3.1 *Let $s > \frac{n}{2}+1$ and $V_0 \in \mathrm{H}^s(\mathbb{R}^n)$. Then $\exists\, T>0$ and $\exists!\, \mathcal{V}^\varepsilon(\tau, X, \theta)$ solution of (21) in $\mathrm{L}^\infty_\tau\left([0,T]; \mathrm{H}^s_{X,\theta}(\mathbb{R}^n \times [0,2\pi])\right)$ such that $\mathcal{V}^\varepsilon(0,X,\theta) = V_0(X)e^{i\theta} + c.c.$.*

Moreover, $\|\mathcal{V}^\varepsilon\|_{\mathrm{L}^\infty_\tau([0,T];\mathrm{H}^s_{X,\theta}(\mathbb{R}^n\times[0,2\pi]))}$ is bounded independantly of ε.

3.2 Application to the Maxwell-Bloch system

System (17) enters the class (18) and can be written as

$$\partial_t V^\varepsilon + A_x \partial_x V^\varepsilon + A_y \partial_y V^\varepsilon + \frac{1}{\varepsilon} L_0 V^\varepsilon + \varepsilon F(V^\varepsilon) = 0, \tag{22}$$

where $V^\varepsilon = (b_x, b_y, e, p, q)$,

$$A_1 = \begin{pmatrix} 0 & 0 & 0 & 0 & 0 \\ 0 & 0 & -1 & 0 & 0 \\ 0 & -1 & 0 & 0 & 0 \\ 0 & 0 & 0 & 0 & 0 \\ 0 & 0 & 0 & 0 & 0 \end{pmatrix}, \quad A_2 = \begin{pmatrix} 0 & 0 & 1 & 0 & 0 \\ 0 & 0 & 0 & 0 & 0 \\ 1 & 0 & 0 & 0 & 0 \\ 0 & 0 & 0 & 0 & 0 \\ 0 & 0 & 0 & 0 & 0 \end{pmatrix},$$

$$L_0 = \begin{pmatrix} 0 & 0 & 0 & 0 & 0 \\ 0 & 0 & 0 & 0 & 0 \\ 0 & 0 & 0 & 0 & -\sqrt{\alpha} \\ 0 & 0 & 0 & 0 & 1 \\ 0 & 0 & \sqrt{\alpha} & -1 & 0 \end{pmatrix} \text{ and } \quad F(V^\varepsilon) = \beta \begin{pmatrix} 0 \\ 0 \\ 0 \\ 0 \\ e\left(p^2+q^2\right) \end{pmatrix}.$$

The characteristic variety is given by

$$\mathrm{Char}(L) = \left\{ (\omega, \mathbf{k}) \in \mathbb{R} \times \mathbb{R}^2, \omega\left(\omega^4 - \omega^2(1+\alpha)|\mathbf{k}|^2\left(1-\omega^2\right)\right) = 0 \right\}. \tag{23}$$

This variety is composed of five branches (*cf* Fig 1, k along the horizontal axis and ω along the vertical axis). The origin is the only singular point of $\mathrm{Char}(L)$.

Remark 3.3 *It is easy to show that, if $(\omega, \mathbf{k})$ belongs to Char(L) and if $\omega \neq 0$, then for all $n \neq \pm 1$, $(n\omega, n\mathbf{k})$ does not belong to the variety (that is, $L(n\omega, n\mathbf{k})$ is invertible).*

From now, one chooses $(\omega, \mathbf{k}) = (\omega, k, 0) \in \mathrm{Char}(L) \setminus \{\omega = 0\}$. Hence, the profile is given by

$$\begin{aligned} V^\varepsilon(t,x,y) &= \mathcal{V}^\varepsilon\left(\varepsilon t, x - \omega'(k)t, y, \frac{kx-\omega t}{\varepsilon}\right) \\ &= \mathcal{V}^\varepsilon(\tau, X, Y, \theta), \end{aligned}$$

where $\omega'(k) = \partial_1 \omega(k,0)$.

The corresponding singular equation reads

$$\left(\varepsilon\partial_\tau - \omega'(k)\partial_X - \frac{\omega}{\varepsilon}\partial_\theta\right)\mathcal{V}^\varepsilon + \frac{1}{\varepsilon}\left(A_x\left(k\partial_\theta + \varepsilon\partial_X\right) + A_Y\left(\varepsilon\partial_Y\right) + L_0\right)\mathcal{V}^\varepsilon + \varepsilon F(V^\varepsilon) = 0, \tag{24}$$

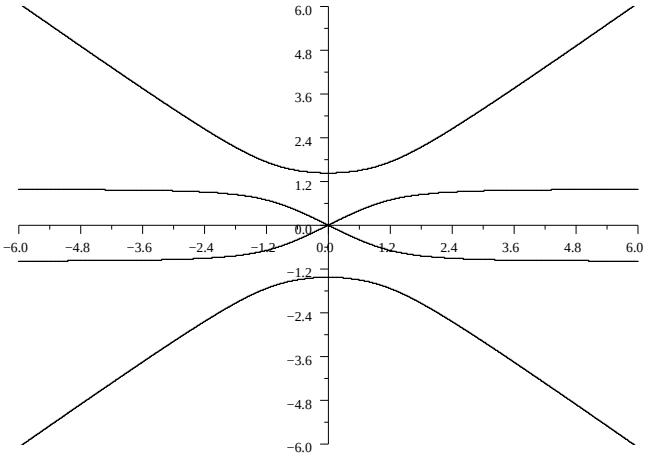

Figure 1: Characteristic variety

with the following initial data:

$$\mathcal{V}^{\varepsilon}(0,X,Y,\theta) = e^{i\theta}V_0(X) + cc. \tag{25}$$

The application of Theorem 3.1 leads to

Corollary 3.1 *For $s > 2$ and $V_0 \in \mathrm{H}^s\left(\mathbb{R}^2\right)$, there exist $T > 0$ independant of ε, and a unique solution $\mathcal{V}^{\varepsilon}\left(\tau, X, Y, \theta\right)$ of (24)-(25) such that $\|\mathcal{V}^{\varepsilon}\|_{\mathrm{L}^{\infty}_{\tau}\left(0,T;\mathrm{H}^{s}_{X,Y,\theta}\right)}$ is bounded independantly of ε.*

3.3 Formal expansion

We will now construct an approximate solution to (24). This will give an approximate solution to the Maxwell-Bloch system:

$$\left\{\begin{array}{rcl} \partial_t b_x &=& -\partial_y e, \\ \partial_t b_y &=& \partial_x e, \\ \partial_t e &=& -\partial_y b_x + \partial_x b_y + \frac{\sqrt{\alpha}}{\varepsilon} q, \\ \partial_t p &=& -\frac{1}{\varepsilon} q, \\ \partial_t q &=& \frac{1}{\varepsilon} p - \frac{\sqrt{\alpha}}{\varepsilon} e + \varepsilon\beta e(p^2+q^2), \end{array}\right. \tag{26}$$

as $\varepsilon \to 0$.

In order to make computations easier, we reduce (26) to a set of two wave equations:

$$\partial_t^2 e = \partial_x^2 e + \partial_y^2 e - \sqrt{\alpha}\partial_t^2 p, \tag{27}$$

$$\partial_t^2 p = -\frac{1}{\varepsilon^2} p + \frac{\sqrt{\alpha}}{\varepsilon^2} e - \beta e\left(p^2 + \varepsilon^2\left(\partial_t p\right)^2\right). \tag{28}$$

We write e and p in terms of profile:

$$e(t,x,y) = E\left(\varepsilon t, x - v_g t, y, \frac{kx-\omega t}{\varepsilon}\right), \tag{29}$$

$$p(t,x,y) = P\left(\varepsilon t, x - v_g t, y, \frac{kx-\omega t}{\varepsilon}\right). \tag{30}$$

The variables of the profile will be respectively denoted by τ, X, Y and θ and the functions are periodic with respect to θ. We expand the profiles in Fourier series with respect to θ, so that the derivatives with respect to t and x acts on the Fourier coefficients of E and P (these ones being denoted by E_j and P_j, $j \in \mathbb{Z}$) in the following manner:

$$\begin{aligned}
\partial_t &\rightarrow \left(-\frac{ij\omega}{\varepsilon}\mathrm{I_d} + \varepsilon\partial_\tau - v_g\partial_X\right),\\
\partial_t^2 &\rightarrow \left(-\frac{ij\omega}{\varepsilon}\mathrm{I_d} + \varepsilon\partial_\tau - v_g\partial_X\right)^2,\\
\partial_x^2 &\rightarrow \left(-\frac{ijk}{\varepsilon}\mathrm{I_d} + \partial_X\right)^2.
\end{aligned}$$

Moreover, we expand E and P with respect to ε, so that, one can write:

$$\begin{aligned}
E &= \sum_{n\geqslant n} \varepsilon^n \left(\sum_{j\in\mathbb{Z}} e^{ij\theta} E_{n,j}\right),\\
P &= \sum_{n\geqslant n} \varepsilon^n \left(\sum_{j\in\mathbb{Z}} e^{ij\theta} P_{n,j}\right).
\end{aligned}$$

We plug the expression of E and P in (27)-(28) and we compute successively the terms of order $O\left(\varepsilon^{-2}\right)$, $O\left(\varepsilon^{-1}\right)$ and $O\left(\varepsilon^{0}\right)$.

- At order $O\left(\varepsilon^{-2}\right)$:

$$-\omega^2 j^2 E_{0,j} = -k^2 j^2 E_{0,j} + \sqrt{\alpha}\omega^2 j^2 P_{0,j}, \tag{31}$$

$$-\omega^2 j^2 P_{0,j} = -P_{0,j} + \sqrt{\alpha} E_{0,j}. \tag{32}$$

  Let us note $\mathcal{D}_j(k,\omega)$ the quantity

$$\mathcal{D}_j(k,\omega) = j^2k^2 - j^2\omega^2\left(1 + \frac{\sqrt{\alpha}}{1-j^2\omega^2}\right).$$

  Then, it is easy to obtain from (31)-(32):

$$\begin{aligned}
P_{0,j} &= \frac{\sqrt{\alpha}}{1-\omega^2 j^2} E_{0,j}, \qquad (33)\\
\mathcal{D}_j(k,\omega) E_{0,j} &= 0.
\end{aligned}$$

  - for $j^2 \neq 1$, $\mathcal{D}_j(k,\omega) \neq 0$ and therefore $E_{0,j}$ is equal to 0 for all θ, τ, X and Y.

– for $j^2 = 1$, we choose k and ω such that $\mathcal{D}_{-1}(k,w) = \mathcal{D}_1(k,w) = 0$. This gives the relation dispersion, which is in our case

$$k^2 = \omega^2 \left(1 + \frac{\sqrt{\alpha}}{1-\omega^2}\right). \tag{34}$$

- At order $O\left(\varepsilon^{-1}\right)$:

$$\begin{aligned} -\omega^2 j^2 E_{1,j} + 2ij\omega c \partial_X E_{0,j} &= -k^2 j^2 E_{1,j} + 2ijkc\partial_X E_{0,j} - \\ &\quad \sqrt{\alpha}\left(-\omega^2 j^2 P_{1,j} + 2ij\omega c \partial_X P_{0,j}\right) \quad (35) \\ -\omega^2 j^2 P_{1,j} + 2ij\omega c \partial_X P_{0,j} &= -P_{1,j} + \sqrt{\alpha} E_{1,j}. \quad (36) \end{aligned}$$

From these two equations, we get

$$\begin{aligned} P_{1,j} &= \frac{1}{1-\omega^2 j^2}\left(\sqrt{\alpha} E_{1,j} - 2ij\omega c \partial_X P_{0,j}\right), \quad (37) \\ \mathcal{D}_j(k,\omega) E_{1,j} &= 2ij\left(k - \omega v_g - \frac{\alpha\omega v_g}{\left(1-\omega^2\right)^2}\right)\partial_X E_{0,j}. \quad (38) \end{aligned}$$

– If $j^2 \neq 1$, as $E_{0,j}$ is equal to 0, then $E_{1,j}$ and $P_{1,j}$ are also equal to 0.

– Otherwise, for $j^2 = 1$, the equation (38) is satisfied if the coefficient of $\partial_X E_{0,j}$ is equal to 0. But equation (34) allows us to easily verify that the group velocity $v_g = \omega'(k)$ satisfies

$$k = \omega v_g \left(1 + \frac{\alpha}{\left(1-\omega^2\right)^2}\right). \tag{39}$$

- At order $O\left(\varepsilon^0\right)$, the non linear effects occur:

$$\begin{aligned} -\omega^2 j^2 E_{2,j} + 2ij\omega c\partial_X E_{1,j} + \left(v_g^2 \partial_X^2 - 2ij\omega\partial_\tau\right) E_{0,j} = \\ -j^2 k^2 E_{2,j} + 2ijk\partial_X E_{1,j} + \left(\partial_X^2 + \partial_Y^2\right) E_{0,j} \\ -\sqrt{\alpha}\left(-\omega^2 j^2 P_{2,j} + \left(v_g^2\partial_X^2 - 2ij\omega\partial_\tau\right) P_{0,j} + 2ij\omega c \partial_X P_{1,j}\right), \quad (40) \end{aligned}$$

$$\begin{aligned} -\omega^2 j^2 P_{2,j} + 2ij\omega c\partial_X P_{1,j} + \left(v_g^2\partial_X^2 - 2ij\omega\partial_\tau\right) P_{0,j} = \\ -P_{2,j} + \sqrt{\alpha} E_{2,j} - \beta F_{0,j}, \quad (41) \end{aligned}$$

where $F_{0,j}$ is the coefficient of $e^{ij\theta}$ in the nonlinearity. It is hence easy to obtain the equations satisfied by $P_{2,j}$ and by $E_{2,j}$ (with (40), (41), (37) and (33)):

$$\left(1-\omega^2\right) P_{2,j} = \sqrt{\alpha} E_{2,j} - 2ij\omega c\partial_X P_{1,j} + \left(2ij\omega\partial_\tau - v_g^2\partial_X^2\right) P_{0,j} - \beta F_{0,j}. \tag{42}$$

$$\begin{aligned} \mathcal{D}_j(k,\omega) E_{2,j} = 2ij\left(k - \omega v_g - \frac{\omega v_g \alpha}{\left(1-\omega^2 j^2\right)^2}\right)\partial_X E_{1,j} + \\ \left(1 - v_g^2 - \frac{v_g^2\alpha}{\left(1-\omega^2 j^2\right)^2} - \frac{4\omega^2 j^2 v_g^2 \alpha}{\left(1-\omega^2 j^2\right)^3}\right)\partial_X^2 E_{0,j} + \partial_Y^2 E_{0,j} + \\ 2ij\omega\left(1 + \frac{\alpha}{\left(1-\omega^2 j^2\right)^2}\right)\partial_\tau E_{0,j} - \frac{\omega^2 j^2\sqrt{\alpha}}{1-\omega^2 j^2}\beta F_{0,j}. \quad (43) \end{aligned}$$

If $j^2 = 1$, then (33) and (39) imply that the right-hand side of (43) is equal to 0, as well as the coefficient of $\partial_X E_{1,j}$. Hence, it only remains the terms involving the partial derivatives of $E_{0,j}$. The coefficient of $\partial_X^2 E_{0,j}$ contains the dispersion of the group velocity (the second derivative of ω), as this one satisfies the equation

$$\frac{k}{v_g}\omega''(k) = 1 - v_g^2 - \frac{v_g^2\alpha}{(1-\omega^2)^2} - \frac{4\omega^2 v_g^2\alpha}{(1-\omega^2)^3}. \tag{44}$$

Finally, the envelop $E_{0,1}$ satisfies the following nonlinear Schrödinger equation:

$$i\partial_\tau E_{0,1} + \frac{1}{2}w''(k)\partial_X^2 E_{0,1} + \frac{v_g}{2k}\partial_Y^2 E_{0,1} = \frac{\omega^2 v_g\alpha}{2k\left(1-\omega^2\right)}\beta F_{0,1}. \tag{45}$$

The nonlinearity $F_{0,1}$ can be easily computed:

$$F_{0,1} = \frac{\left(3+\omega^2\right)\alpha}{\left(1-\omega^2\right)^2}\left|E_{0,1}\right|^2 E_{0,1}. \tag{46}$$

We use (46) in (45) to obtain the nonlinear Schrödinger equation which is satisfied by the envelop $\mathcal{E} = E_{0,1}$:

$$i\partial_\tau \mathcal{E} + \frac{1}{2}w''(k)\partial_X^2 \mathcal{E} + \frac{v_g}{2k}\partial_Y^2 \mathcal{E} = \frac{\omega^2\left(3+\omega^2\right)v_g\alpha^{\frac{3}{2}}}{2k\left(1-\omega^2\right)^3}\beta\left|\mathcal{E}\right|^2\mathcal{E}. \tag{47}$$

Let us fix now $s \geqslant 1$ and $E_0 \in \mathrm{H}^s\left(\mathbb{R}^2\right)$. There exists $T_0 > 0$ such that there exists a unique solution $\mathcal{E}\left(\tau, X, Y\right)$ of (47) such that $\mathcal{E}\left(0, X, Y\right) = E_0(X, Y)$. Thanks to $\mathcal{E}$, one constructs an approximate solution of (26) as follows:

Take $E_{0,1} = \mathcal{E}$, $B_{x\ 0,1} = 0$, $B_{y\ 0,1} = -\frac{k}{\omega}\mathcal{E}$, $P_{0,1} = \frac{\sqrt{\alpha}}{1-\omega^2}\mathcal{E}$ and $Q_{0,1} = \frac{i\omega\sqrt{\alpha}}{1-\omega^2}\mathcal{E}$. We construct an approximate solution

$$\mathcal{W}\left(\tau, X, Y, \theta\right) = \left(B_{x\ 0,1}, B_{y\ 0,1}, E_{0,1}, P_{0,1}, Q_{0,1}\right)e^{i\theta} + c.c. \tag{48}$$

To construct the initial condition, we choose $E_0 \in \mathrm{H}^s$ and we consider $V_0(X, Y) = \left(0, -\frac{k}{\omega}, 1, \frac{\sqrt{\alpha}}{1-\omega^2}, \frac{i\omega\sqrt{\alpha}}{1-\omega^2}\right)E_0(X, Y)$.

Theorem 3.2 *Let s be large enough. There exist $T_1 > 0$ and a unique $\mathcal{V}^\varepsilon\left(\tau, X, Y, \theta\right) \in \mathcal{C}\left(\left[0, T_1\right]; \mathrm{H}^s\left(\mathbb{R}^2 \times [0, 2\pi]\right)\right)$ solution of (24), and $C > 0$ such that*

$$\sup_{\tau\in[0,T_1]} \left\|\mathcal{V}^\varepsilon - \mathcal{W}\right\|_{\mathrm{H}^s_{X,\theta}(\mathbb{R}^2\times[0,2\pi])} \leqslant C\varepsilon.$$

Of course, this result can be expressed in terms of the original variables in L^∞ norm:

Theorem 3.3 *Let V^ε be the solution of (22). Then,*

$$\sup_{\left[0,\frac{T_1}{\varepsilon}\right]\times\mathbb{R}^2} \left|V^\varepsilon(t, x, y) - \mathcal{W}\left(\varepsilon t, x - \omega'(k)t, y, \frac{kx - \omega t}{\varepsilon}\right)\right| \leqslant C\varepsilon.$$

Higher order expansions can be done and one can search for a solution $\mathcal{V}^\varepsilon\left(\tau, X, Y, \theta\right)$ under a serie

$$\mathcal{V}^\varepsilon\left(\tau, X, Y, \theta\right) = \sum_{n=0}^{p} \varepsilon^n \mathcal{W}^n\left(\tau, X, Y, \theta\right) + O\left(\varepsilon^{p+1}\right). \tag{49}$$

The functions $\left(\mathcal{W}^n\right)_{n\geqslant 1}$ are then given in terms of $\mathcal{W}$.

4 Numerical schemes

In section 3, we have detailed the tools that we will use for the validation of our numerical results. In particular, we will compare the solution of the Maxwell-Bloch system (17) and its envelop (given by (47)). We will first briefly describe a classical numerical scheme for the nonlinear Schrödinger (NLS) equation, then we will explain the proposed scheme for the Maxwell-Bloch system.

We will suppose that all the functions are periodic in the space domain so that we could use the discrete Fourier transform. Let $u(X,Y)$ be a function whose period is (T_X, T_Y). The discretization points are:

$$\begin{aligned} X_k &= \frac{kT_X}{N_X},\ k \in \{0, \cdots, N_X - 1\}, \\ Y_l &= \frac{lT_Y}{N_Y},\ l \in \{0, \cdots, N_Y - 1\}, \end{aligned}$$

where N_X and N_Y are the number of points. Then the discrete Fourier transform of u (denoted by $\hat{u}$) is such that

$$u(X_k, Y_l) = \sum_{k=-\frac{N_X}{2}}^{\frac{N_X}{2}-1} \sum_{l=-\frac{N_X}{2}}^{\frac{N_X}{2}-1} \hat{u}(k,l) e^{\frac{2i\pi k}{T_X}X} e^{\frac{2i\pi l}{T_Y}Y}.$$

4.1 Numerical scheme for the NLS equation

In order to solve numerically the NLS equation, we use a classical splitting method (*cf* [18] et [17]), which is of order 2 in time (*cf* [2]). Let

$$i\partial_\tau u = -\lambda \partial_X^2 u - \mu \partial_Y^2 + \nu |u|^2 u, \tag{50}$$

be the NLS equation (λ, μ and ν are three real numbers, which will be given by (47) for the numerical tests). We denote by $\exp(L_{\text{NLS}})(\tau)u_0$ and $\exp(NL_{\text{NLS}})(\tau)u_0$ the solution of respectively

$$\begin{cases} \partial_\tau u &= L_{\text{NLS}} u, \\ u(\tau = 0) &= u_0, \end{cases}$$

and

$$\begin{cases} \partial_\tau u &= NL_{\text{NLS}} u, \\ u(\tau = 0) &= u_0, \end{cases}$$

at time τ, where

$$\begin{aligned} L_{\text{NLS}} u &= i\lambda \partial_X^2 u + i\mu \partial_Y^2 u, \\ NL_{\text{NLS}} u &= -i\nu |u|^2 u. \end{aligned}$$

The splitting works as follows: knowing $u(\tau)$, we compute $u(\tau + \Delta\tau)$ in three steps:

- $u_1\left(\tau + \frac{\Delta\tau}{2}\right) = \exp(L_{\text{NLS}})(\frac{\Delta\tau}{2})u(\tau)$.
- $u_2(\tau + \Delta\tau) = \exp(NL_{\text{NLS}})(\Delta\tau)u_1\left(\tau + \frac{\Delta\tau}{2}\right)$.
- $u(\tau + \Delta\tau) = \exp(L_{\text{NLS}})(\frac{\Delta\tau}{2})u_2(\tau + \Delta\tau)$.

The computation of the first and third steps are done with the help of the discrete Fourier transform:

$$\widehat{u_1}\left(\tau+\frac{\Delta\tau}{2}\right)(k,l)=\exp\left(-i\Delta\tau\left(\lambda\left(\frac{2\pi k}{T_X}\right)^2+\mu\left(\frac{2\pi l}{T_Y}\right)^2\right)\right)\hat{u}(k,l).$$

The computation of the second one is easily done, since, if u is a solution to $i\partial_\tau u = \nu|u|^2 u$ on $[\tau;\tau+\Delta\tau]$, then $|u|^2(t)$ is constant. This equation can then be solved exactly.

4.2 Numerical scheme for the Maxwell-Bloch equations

In order to construct a numerical solution to the Maxwell-Bloch system, we will discretize the singular equation (21), as in [6]. Here we use a spectral method: consider $\mathcal{V}^\varepsilon(\tau,X,Y,\theta)$ the solution to

$$\left(\varepsilon\partial_\tau-\nabla\omega.\nabla_{\mathbf{X}}-\frac{\omega}{\varepsilon}\partial_\theta\right)\mathcal{V}^\varepsilon(\tau,\mathbf{X},\theta)+\frac{1}{\varepsilon}\left(A\left(\varepsilon\partial_{\mathbf{X}}+\mathbf{k}\partial_\theta\right)+L_0\right)\mathcal{V}^\varepsilon(\tau,\mathbf{X},\theta)=\varepsilon F\left(\mathcal{V}^\varepsilon(\tau,\mathbf{X},\theta)\right),\quad(51)$$

with $\mathcal{V}^\varepsilon(\tau,X,Y,\theta)=\sum_{j\in\mathbb{Z}}{\mathcal{V}^\varepsilon}_j e^{ij\theta}$. The (infinite) system of equations satisfied by ${\mathcal{V}^\varepsilon}_j$ is

$$\left(\varepsilon\partial_\tau-\omega'(k)\partial_X-\frac{ij\omega}{\varepsilon}\mathrm{I_d}\right){\mathcal{V}^\varepsilon}_j+\left(A_1\left(\partial_X+\frac{ijk}{\varepsilon}\right)+A_2\partial_Y+\frac{1}{\varepsilon}L_0\right){\mathcal{V}^\varepsilon}_j=\varepsilon P_j\left(F(V^\varepsilon)\right),\quad(52)$$

for $j\in\mathbb{Z}$. The operator P_j is the orthogonal projector on the j^{th} Fourier mode: $(P_j f)=\frac{1}{2\pi}\int_0^{2\pi} f(\theta)e^{-ij\theta}\mathrm{d}\theta$.

We are lead to an infinite system of PDE's that we will truncate. We now explain how we integrate each of the equation included in (52). The eigenvalues of the linear part of (52) are purely imaginary and can be of order ε^{-2}. In order to explain our scheme, let us consider the following example:

$$\left\{\begin{array}{rcl} y'(t)+\frac{i}{\varepsilon^2}y(t) &=& f(t),\\ y(0) &=& 0.\end{array}\right.$$

In this equation, f is some source term. When ε tends to 0, the asymptotic solution is of order $\varepsilon^2 f$. As usual, splitting on this equation gives a solution of size $\Delta t f$ after the first time step, which is completely different from the size of the asymptotic solution (unless $\Delta t\leqslant\varepsilon^2$, which is quite restrictive). We therefore adopt another strategy in order to keep this order of magnitude. We use an exponential scheme thanks to the Duhamel formula: if Δt is the time step,

$$y(t+\Delta t)=e^{i\frac{\Delta t}{\varepsilon^2}}y(t)+\int_0^{\Delta t}e^{\frac{i}{\varepsilon^2}(\Delta t-s)}f(t+s)\mathrm{d}s.$$

We approximate $f(t+s)$ by $f(t)$ and get:

$$y(t+\Delta t)=e^{i\Delta t\varepsilon^{-2}}y(t)+\frac{\varepsilon^2}{i}\left(e^{i\Delta t\varepsilon^{-2}}-1\right)f(t).$$

We apply the method to our system: by denoting by $S(\tau)$ the semi-group associated to the linear part of (52) and $\mathcal{V}_j^n = \mathcal{V}_j(n\Delta\tau)$, (52) becomes

$$\mathcal{V}_j^{n+1} = S(\Delta\tau)\mathcal{V}_j^n + \int_0^{\Delta\tau} S(\Delta\tau - s)P_j(F(\mathcal{V}(\tau+s)))\mathrm{d}s. \tag{53}$$

We approximate $F(\mathcal{V}(\tau+s))$ by $F(\mathcal{V}^\varepsilon(\tau))$ in order to have an explicit method:

$$\mathcal{V}_j^{n+1} = S(\Delta\tau)\mathcal{V}_j^n + \left(\int_0^{\Delta\tau} S(\Delta\tau - s)\mathrm{d}s\right) P_j(F(\mathcal{V}^n)). \tag{54}$$

Now, the easiest way to compute $S(\Delta\tau)$ is to use a spectral method.

Linear part: spectral method If χ and η denote the Fourier dual variables of respectively X and Y, we denote by

$$\alpha_1 = \frac{2\pi}{T_X}\chi + \frac{jk}{\varepsilon}, \tag{55}$$

$$\alpha_2 = \frac{2\pi}{T_Y}\eta, \tag{56}$$

$$\gamma = v_g\frac{2\pi}{T_X}\chi + \frac{j\omega}{\varepsilon}. \tag{57}$$

The action of the group $S(\Delta\tau)$ is then given by:

$$\widehat{S(\Delta\tau)u}(\chi,\eta) = \exp\left(i\alpha_1 A_1 + i\alpha_2 A_2 + \frac{1}{\varepsilon}L_0 + i\gamma \mathrm{I_d}\right)\hat{u}(\chi,\eta). \tag{58}$$

We consider now a diagonal form of the matrix $i\alpha_1 A_1 + i\alpha_2 A_2 + \frac{1}{\varepsilon}L_0$. We have to deal with two cases:

- $\alpha_1 = \alpha_2 = 0$

  In this case, 0 is an eigenvalue of order 3, the two other eigenvalues are $\pm\frac{j}{\varepsilon}\sqrt{\alpha+1}$.

- $\alpha_1 \neq 0$ or $\alpha_2 \neq 0$

  In this case, 0 is simple, the four other eigenvalues are roots of

  $$T^2\left(1+\alpha+\varepsilon^2T^2\right) + \left(\alpha_1^2+\alpha_2^2\right)\left(1+\varepsilon^2T^2\right) = 0$$

  and, of course, are purely imaginary numbers.

The effective computation of $S(\Delta\tau)$ is done by using the discrete Fourier transform.

Nonlinearity The nonlinear part $P_j(F(W(\tau)))$ is computed explicitely, with the help of (52).

We can remark that the number of harmonics that we take into account in (54) is penalizing in computation time. But

- the coefficients of the equation (26) being real numbers, $\mathcal{W}_{-j} = \overline{\mathcal{W}_j}$. Thus we compute (54) only for positive integers j,

- the nonlinearity being of order 3, all even harmonics are equal to zero (*cf* section 3): at $\tau = 0$, the signal is monochromatic),
- it is useless to compute too much harmonics: the asymptotic expansion in Section 3 shows that the third harmonic is of order ε^2, which is very small even if ε is not so small.

5 Numerical results in the one dimensional case

We present in this section the numerical results obtained for the Maxwell-Bloch equations (*cf* 4.2) and for the NLS equation (*cf* 4.1) in one space dimension. We restrict ourself to the case where the only harmonics that are considered are $\left(e^{ij\theta}\right)$, $j \leqslant 3$. Following the remark done at the end of Section 4, that means that one has to consider only $j = 1$ and $j = 3$.

In the one dimensional case, the numerical scheme for the Maxwell-Bloch equation becomes:

$$\mathcal{V}_j^{n+1} = S(\Delta\tau)\mathcal{V}_j^n + \varepsilon \left(\int_0^{\Delta\tau} S(\Delta\tau - s)\mathrm{d}s \right) P_j(F(\mathcal{V}(\tau))), \tag{59}$$

for $j = 1, 3$, with

$$\widehat{S(\Delta\tau)\mathcal{V}_j^n}(\chi) = \exp\left(i\alpha_1 A_1 \frac{1}{\varepsilon} L_0 + i\gamma \mathrm{I_d} \right) \widehat{\mathcal{V}_j^n}(\chi),$$

and α_1 and γ given by (55) et (57). The nonlinearity $P_j(F(\mathcal{V}(\tau)))$ is computed as explained in section 4.2.

The NLS equation reads

$$i\partial_\tau u = -\frac{1}{2}\omega''(k)\partial_X^2 u + \frac{\omega^2\left(3+\omega^2\right) v_g \alpha^{\frac{3}{2}}}{2k\left(1-\omega^2\right)^3}\beta\left|u\right|^2 u \tag{60}$$

(*cf* 4.1). The group velocity and $\omega''(k)$ are respectively given by (39) and (44).

The physical parameters α and β which appear in $S(\Delta\tau)$ are of order 1. In this section, for the sake of simplicity, they will be taken equal to 1.

The initial datum (at $\tau = 0$) is

$$\begin{aligned} \mathcal{V}_1^0(0, X) &= e^{-46X^2} \text{ for } X \in [0, 1] \\ \mathcal{V}_3^0(0, X) &= 0, \end{aligned}$$

and we compute the solutions for $\tau \in [0, 1]$.

5.1 Numerical convergence with respect to the number of modes for space discretization

Recall that the component e of the electric field solution to (26) is given in term of a profile E^ε thanks to (27). This profile $E^\varepsilon(\tau, X, Y, \theta)$ can be expanded in Fourier series $E^\varepsilon(\tau, X, Y, \theta) = \sum_{j\in\mathbb{Z}} E_j^\varepsilon(\tau, X, Y)\, e^{ij\theta}$. Our numerical method consists precisely in computing an approximation of $E_j^\varepsilon(\tau, X, Y)$ for $j = 1$ and 3.

Now, if u is a solution to the NLS equation, Theorem 3.2 precisely states that

$$\sup_{\tau\in[0,T_1]} \|E_1^\varepsilon(\tau,X,Y) - u(\tau,X,Y)\|_{\mathrm{H}^s_{X,\theta}(\mathbb{R}^2\times[0,2\pi])} \leqslant C\varepsilon.$$

In order to validate our method in 1D, we will compare the numerical results for E^ε and u. For the numerical tests of the numerical convergence, $\varepsilon = \Delta\tau =$ 1E-3. We take successively 64, 128, 256 and 1024 modes for the space discretization. The influence of the number of points is very low.

In Figure 2, we have plotted the real part of E_1^ε at time $\tau = 0.5$ for 64 Fourier modes. We have computed the successive relative errors between the solutions with 64 and 128 modes, then between 128 and 256, then between 256 and 1024 in L^2 norm. The results are summarized in the following table:

Compared N_X	64-128	128-256	256-1024
Relative error	4.23E-7	1.25E-7	4.97E-8

Figure 3 shows the evolution for $\tau \in [0,1]$ of the L^∞ norm of the real part of the first harmonic E_1 for 64 Fourier modes.
We have performed the same kind of tests with the Schrödinger equation. We have computed the successive relative errors between the solutions with 64 and 128 modes, then between 128 and 256, then between 256 and 1024 in L^2 norm. The results are summarized in the following table:

Compared N_X	64-128	128-256	256-1024
Relative error	3.3E-7	1.2E-7	4.5E-8

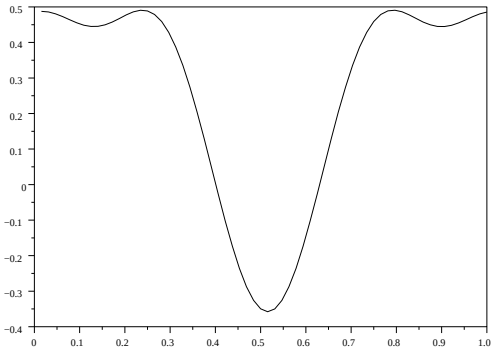

Figure 2: Real part of the first harmonic of the electric field e of the Maxwell-Bloch system (26), at $\tau = 0.5$, for $N_X = 64$ Fourier modes

A few points are therefore sufficient to achieve a good accuracy.

The computations have been performed on a processor Sun Fire 4800 1 Ghz. The computation time, with respect to the number of points is given by the following table:

N_X	64	128	256	1024
Time	5s	10s	22s	1mn 39s

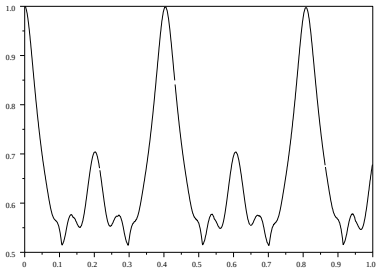

Figure 3: Evolution of the L^∞ norm of the real part of the first harmonic of the electric field e solution to the Maxwell-Bloch system (26), with respect to time, for $NX = 64$ Fourier modes

5.2 Numerical convergence with respect to the time step

In this section, we fix $N_X = 128$ and $\varepsilon = 1E-3$. We compute successively the real part of the electric field e at time $\tau = 0.5$ for different time steps : Δt=1E-1, 1E-2, 1E-3 and 1E-4. The relative errors between the solutions with Δt=1E-1 and 1E-2, between the solutions with Δt=1E-2 and 1E-3, between the solutions with Δt=1E-3 and 1E-4, in L^2 norm are:

Compared Δt	1E-1/1E-2	1E-2/1E-3	1E-3/1E-4
Relative error	0.045	0.007	0.0009

The scheme is certainly not of order 2.

5.3 Influence of the time step for MB, with respect to NLS

The scheme that solves the Maxwell-Bloch equations computes explicitly the semi-group $S(\Delta\tau)$ (*cf* (58)). When an eigenvalue of $i\alpha_1 A_1 + \frac{1}{\varepsilon}L_0 + i\gamma \mathrm{I_d}$ is very small, the integral

$$\int_0^{\Delta\tau} e^{\lambda(\Delta\tau - s)} \mathrm{d}s = \frac{1}{\lambda}\left(e^{\lambda(\Delta\tau)} - 1\right)$$

is of order $\Delta\tau$.

As this case occurs, if $\Delta\tau$ is not of order ε, the numerical error will be larger than ε and the relative error between the solution to the Maxwell-Bloch system and the one given by the NLS equation could be larger than ε.

On the contrary, as soon as the time step becomes sufficiently small, ($\Delta\tau \leqslant \varepsilon$), the numerical relative error respects those of the theory. Hence, it is useless to choose $\Delta\tau$ less than ε in order to increase the precision. Figures 4, 5 and 6 for N_X=128 and ε =1E-1, 1E-2 nd 1E-3 respectively, show the relative error (plotted with respect to time $\tau \in [0, 1]$) between the real part of the solution to the NLS equation and the real part of the first harmonic E_1 of the electric field of the Maxwell-Bloch system. According to (49), this error should be of order ε, if $\Delta\tau \leqslant \varepsilon$.

For ε =1E-1, as $\Delta\tau \leqslant \varepsilon$ for all chosen $\Delta\tau$, the relative error is of order ε. When we decrease ε to 1E-2, we find again the behavior described above, as we can see on Figures 5 (a), (b) and (c). On Figure (a), we see that the error is of order 0.1, which

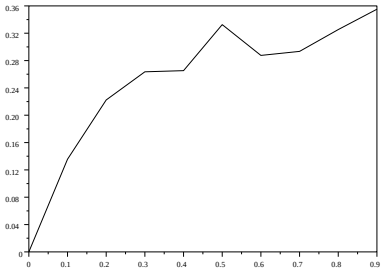

(a) $\Delta\tau$ = 1E-1

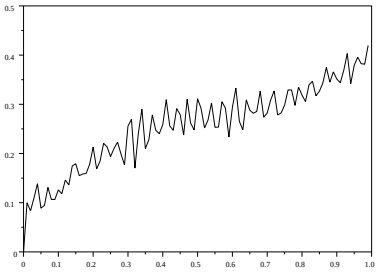

(b) $\Delta\tau$ = 1E-2

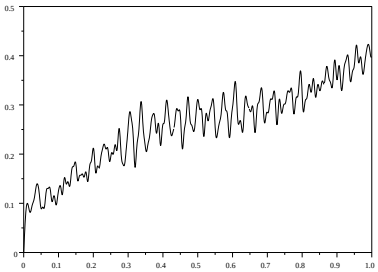

(c) $\Delta\tau$ = 1E-3

Figure 4: Relative error with respect to time in L^∞ norm between the real part of the first harmonic of the electric field given by the Maxwell-Bloch system and the solution to the NLS equation. Numerical convergence in terms of the time step. $N_X = 128$, with ε = 1E-1

is the value of $\Delta\tau > \varepsilon$. On Figures (b) and (c), as $\Delta\tau \leqslant \varepsilon$, the error decreases and stays to ε. And if we set ε =1E-3, we can see the results on Figures 6 (a), (b), (c) and (d). On Figure (d), we have chosen a very small value of $\Delta\tau$ ($\Delta\tau = 1E-5$), and the error stays of course at level ε. Hence we can chose an optimal time step for our scheme, which is $\Delta\tau = \varepsilon$.

The computation time, with respect to the time step is given by the following table (N_X =128 and ε = 1E-3):

$\Delta\tau$	1E-1	1E-2	1E-3	1E-4
Time	1s	1s	10s	1mn 44s

5.4 Comparison with NLS: validation of the asymptotic behavior

We fix again N_X=128 and $\Delta\tau = \varepsilon$ and we compare the Maxwell-Bloch solution with the NLS solution. Theorem 3.2 shows that the error between these solutions has an order of magnitude of ε. Figures 7 (a), (b) and (c) show the relative error for (respectively) ε=1E-3, 1E-4 and 1E-5. The error is of order ε for each of these

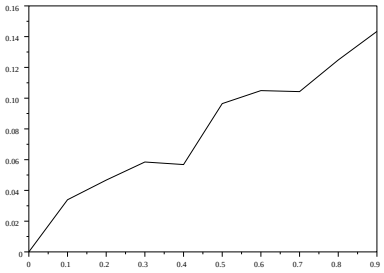

(a) $\Delta\tau = 1\text{E-}1$

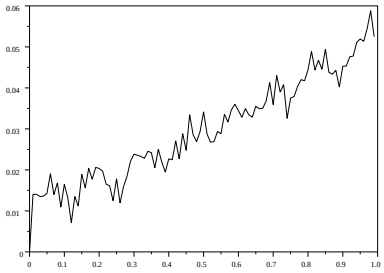

(b) $\Delta\tau = 1\text{E-}2$

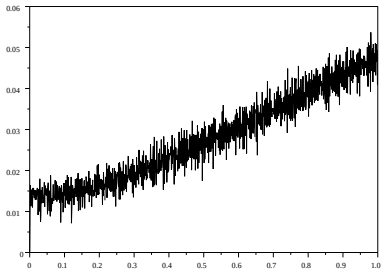

(c) $\Delta\tau = 1\text{E-}3$

Figure 5: Relative error with respect to time in L^∞ norm between the real part of the first harmonic of the electric field given by the Maxwell-Bloch system and the solution to the NLS equation. Numerical convergence in terms of the time step. $N_X = 128$, with $\varepsilon = 1\text{E-}2$

cases. If we decrease the number of points ($N_X = 64$), the same behavior occurs, as we can see in Figures 8 (a), (b) and (c).

5.5 Polarization and third harmonic

In the previous section, we have compared the real part of the first harmonic with the solution to the NLS equation. Now we come back to the solution of the Maxwell-Bloch system (26).

Now we remark that the approximate solution for the first harmonic, given by (48) is parallel to the constant vector $\left(0, -\frac{k}{\omega}, 1, \frac{\sqrt{\alpha}}{1-\omega^2}, \frac{i\omega\sqrt{\alpha}}{1-\omega^2}\right)$, which is called the polarization vector. If $\Pi(k)$ denotes the orthogonal projector onto the vector-space spanned by this vector, the convergence result 3.2 implies that $(\mathrm{I_d} - \Pi(k))\, E_1$ is of order ε.

Concerning the third harmonic, Theorem 3.2 implies that E_3 is of order ε^2. The aim of this section is to check numerically these two orders of magnitude.

Figure 9 shows the relative error between E_1 and the polarization of E_1, $\Pi(k)E_1$,

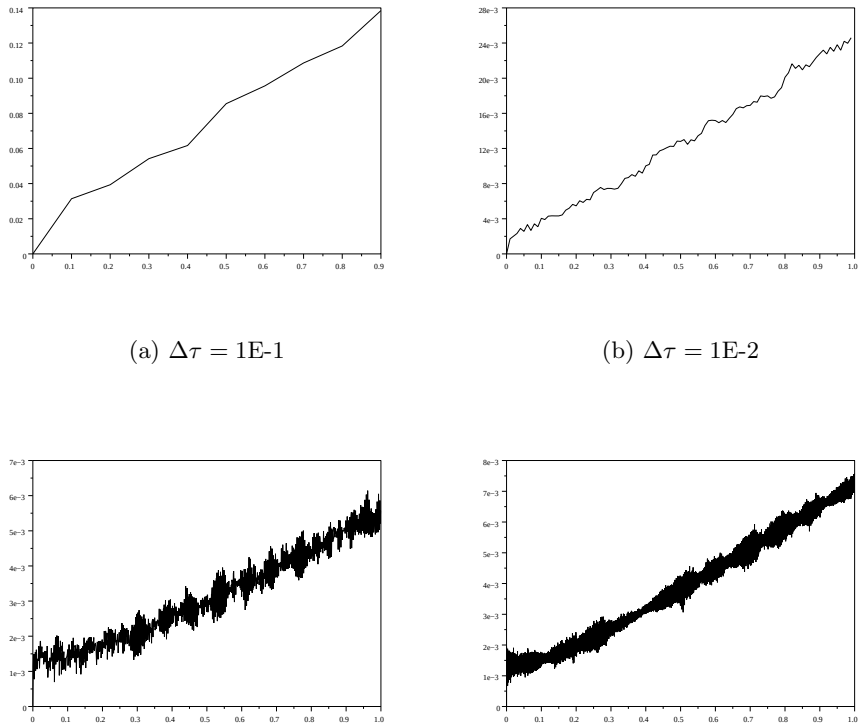

(a) $\Delta\tau$ = 1E-1

(b) $\Delta\tau$ = 1E-2

(c) $\Delta\tau$ = 1E-3

(d) $\Delta\tau$ = 1E-5

Figure 6: Relative error with respect to time in L^∞ norm between the real part of the first harmonic of the electric field given by the Maxwell-Bloch system and the solution to the NLS equation. Numerical convergence in terms of the time step. $N_X = 128$, with ε = 1E-3

that is $\tau \mapsto \frac{|(\mathrm{I_d}-\Pi(k))E_1|_\infty}{|E_1|_\infty}$, for $\tau \in [0,1]$, with $\varepsilon = \Delta\tau$ =1E-3 and N_X=128.

Decreasing the number of points does not change the order of magnitude of this error, as we can see in Figures 10 (a) and (b) (N_X=64).

Figure 11 (a) and (b) show the L^∞ norm of the third harmonic, for $N_X = 128$ and (respectively) $\Delta\tau = \varepsilon$ = 1E-3 and 1E-4.

If we decrease the number of points to 64, the order of magnitude is always of order ε (see Figures 12 (a) and (b)).

6 Numerical results in the two dimensional case

We present now the two dimensional case. The numerical schemes are those given by (54) for the Maxwell-Bloch equations, and in section 4.1 for the NLS equation. As in the one dimension case, α and β are taken equal to 1.

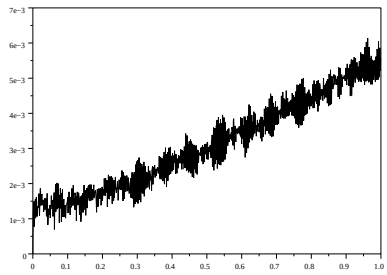

(a) $\Delta\tau = \varepsilon =$ 1E-3

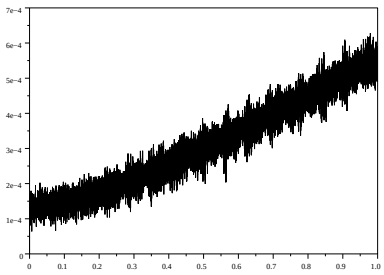

(b) $\Delta\tau = \varepsilon =$ 1E-4

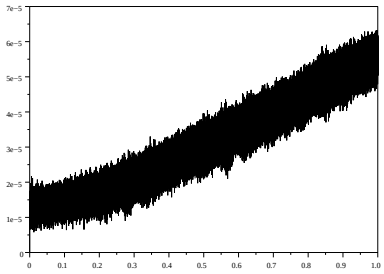

(c) $\Delta\tau = \varepsilon =$ 1E-5

Figure 7: Relative error with respect to time in L^∞ norm between the real part of the first harmonic of the electric field given by the Maxwell-Bloch system and the solution to the NLS equation. Convergence for several values of ε. $N_X = 128$ and $\Delta\tau = \varepsilon$

The functions are periodic and the initial data is

$$\begin{aligned} \mathcal{W}_1^0(0, X, Y) &= e^{-46\left(X^2+Y^2\right)} \text{ for } X, Y \in [0, 1] \\ \mathcal{W}_3^0(0, X, Y) &= 0. \end{aligned}$$

The tests are done for $\tau \in [0, 1]$. The number of points in the X and Y directions are the same : $N_X = N_Y$.

6.1 Numerical convergence with respect to the number of modes for space discretization

The results are the same as in the one dimensional case: no difference is noticed when we choose a number of points equal to 32, 64, 128, 256 or 512. The figures presented are a section at $Y = 0.5$ for 64. The figure 13 shows a section of the real part of the first harmonic of the component of the electric field at $\tau = 0.5$.

The figure 14 shows the same section of the solution of the NLS equation, at $\tau = 0.5$, for 64 Fourier modes. Finally, the evolution of the L^∞ norm of the solution

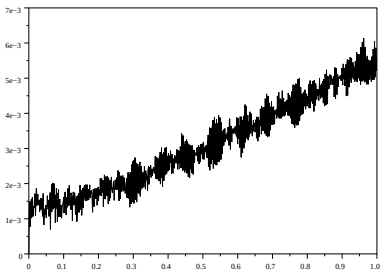

(a) $\Delta\tau = \varepsilon =$ 1E-3

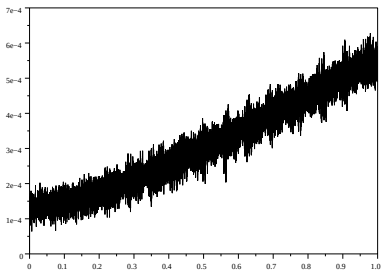

(b) $\Delta\tau = \varepsilon =$ 1E-4

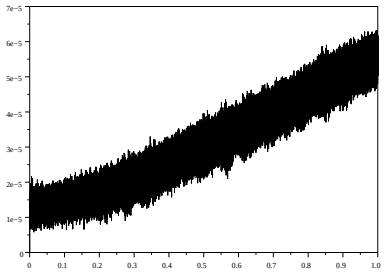

(c) $\Delta\tau = \varepsilon =$ 1E-5

Figure 8: Relative error with respect to time in L^∞ norm between the real part of the first harmonic of the electric field given by the Maxwell-Bloch system and the solution to the NLS equation. Convergence for several values of ε. $N_X = 64$ and $\Delta\tau = \varepsilon$

of the Maxwell-Bloch system is shown in figure 15 for N_X =64.

We have computed the successive relative errors between the solutions with 64 and 128 modes (in each direction), then between 128 and 256, then between 256 and 1024 in L^2 norm. The results are summarized in the following table:

Compared $N_X = N_Y$	32-64	64-128	128-256	128-512
Relative error	1.59E-6	6.34E-7	2.15E-7	7.67E-8

The computations have been performed on a processor Sun Fire 4800 1 Ghz. The computation time, with respect to the number of points, is given by the following table:

$N_X = N_Y$	32	64	128	256
Time	36s	2mn 47s	20mn 8s	3h 11mn

6.2 Numerical convergence with respect to the time step

In this section, we fix $N_X = 128$ and $\varepsilon = 1E-3$. We compute successively the real part of the electric field e at time $\tau = 0.5$ for different time steps : Δt=1E-1, 1E-2,

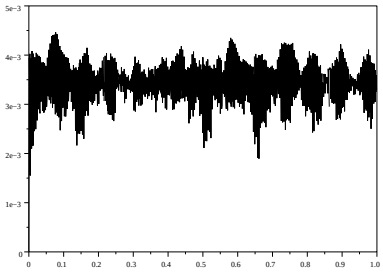

(a) $\Delta\tau = \varepsilon =$ 1E-3

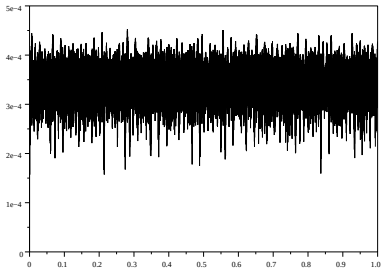

(b) $\Delta\tau = \varepsilon =$ 1E-4

Figure 9: Relative error between the polarized solution and the solution (*i.e.* $\frac{|(\mathrm{I_d} - \Pi(k))E_1|_\infty}{|E_1|_\infty}$) with respect to $\tau \in [0, 1]$), with $N_X = 128$

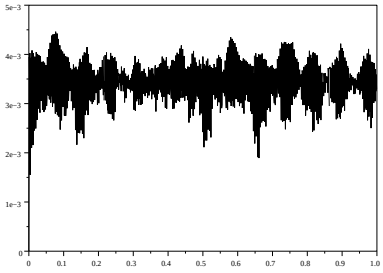

(a) $\Delta\tau = \varepsilon =$ 1E-3

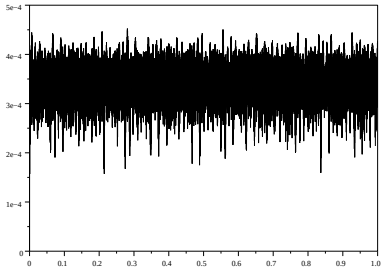

(b) $\Delta\tau = \varepsilon =$ 1E-4

Figure 10: Relative error between the polarized solution and the solution (*i.e.* $\frac{|(\mathrm{I_d} - \Pi(k))E_1|_\infty}{|E_1|_\infty}$) with respect to $\tau \in [0, 1]$), with $N_X = 64$

1E-3 and 1E-4. The relative error of these solutions is given by the following table:

Compared Δt	1E-1/1E-2	1E-2/1E-3	1E-3/1E-4
Relative error	0.03	0.0048	0.0005

6.3 Influence of the time step for MB, with respect to NLS

The same phenomenons as in the one dimensional case appear:

- When $\Delta\tau$ is larger than ε, the relative error between the solution of Maxwell-Bloch and of NLS is larger than ε. Hence, the scheme does not respect the theoretical expansion (49).
- When $\Delta\tau$ is smaller than ε, the order of magnitude of the relative error between the solution of Maxwell-Bloch and of NLS is of ε. Thus, it is again useless to

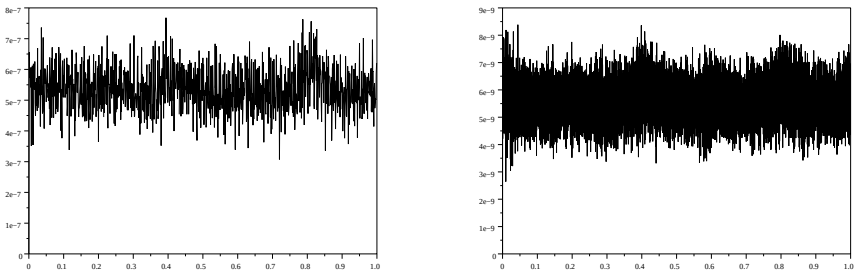

(a) $\Delta\tau = \varepsilon =$ 1E-3 (b) $\Delta\tau = \varepsilon =$ 1E-4

Figure 11: L^∞ norm of the third harmonic of the solution to the Maxwell-Bloch system with respect to time, with $N_X = 128$

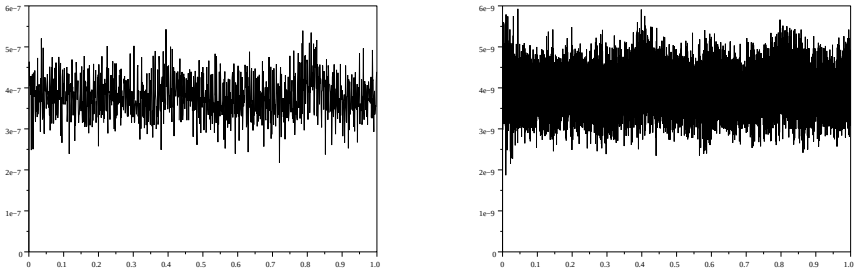

(a) $\Delta\tau = \varepsilon =$ 1E-3 (b) $\Delta\tau = \varepsilon =$ 1E-4

Figure 12: L^∞ norm of the third harmonic of the solution to the Maxwell-Bloch system with respect to time, with $N_X = 64$

choose too small time steps and the scheme allows us to choose an optimal time step, which is equal to ε.

Figures 16 (a), (b) and (c) show a comparison of the relative error for different time steps, for $N_X = N_Y = 128$ and $\varepsilon =$1E-1. On Figure (a), the time step is less than ε, and the error is greater than ε, and is of order $\Delta\tau$. And on Figures (b) and (c), when $\Delta\tau \leqslant \varepsilon$, the error is of order ε. When we decrease ε to 1E-2, we find again the behavior described above, as we can see on Figures 17 (a), (b) and (c). And if we set $\varepsilon =$1E-3, we can see the results on Figures 18 (a), (b), (c) and (d). On Figure (d), we have chosen a very small value of $\Delta\tau$ ($\Delta\tau = 1E-5$), and the error stays of size ε.

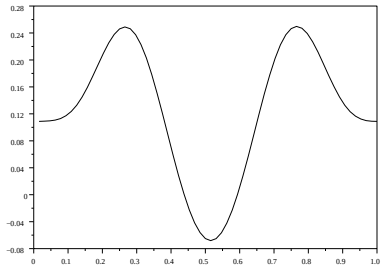

Figure 13: Real part of the first harmonic of the electric field e of the 2D Maxwell-Bloch system (26), at $\tau = 0.5$, for $N_X = N_Y = 64$ Fourier modes. Section at $Y = 0.5$

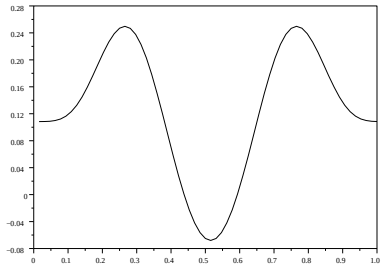

Figure 14: Real part of the solution of the NLS equation (50), at $\tau = 0.5$, for $N_X = N_Y = 64$ Fourier modes. Section at $Y = 0.5$

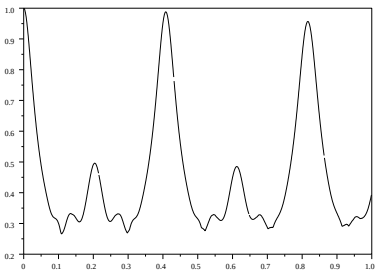

Figure 15: Evolution of the L^∞ norm of the real part of the first harmonic of the electric field e solution to the 2D Maxwell-Bloch system (26), with respect to time, for$N_X = N_Y = 64$ of Fourier modes

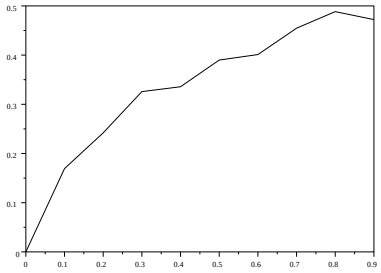

(a) $\Delta\tau$ = 1E-1

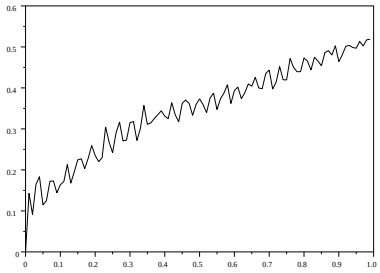

(b) $\Delta\tau$ = 1E-2

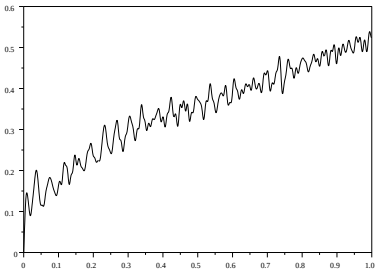

(c) $\Delta\tau$ = 1E-3

Figure 16: Relative error with respect to time in L^∞ norm between the real part of the first harmonic of the electric field given by the Maxwell-Bloch system and the solution to the NLS equation. Numerical convergence in terms of the time step. $N_X = N_Y = 128$, with ε = 1E-1

The computation time, with respect to the time step is given by the following table ($N_X = N_Y$ =128 and ε = 1E-3):

$\Delta\tau$	1E-1	1E-2	1E-3	1E-4
Time	25s	2mn 17s	20mn 8s	3h 27mn

6.4 Comparison with NLS: validation of the asymptotic behavior

We fix again $N_X = N_Y = 128$ and $\Delta\tau = \varepsilon$ for those tests. The relative error of the L^2 norm between Maxwell-Bloch and NLS is of order ε. The figures show this for ε=1E-3, and the figures 19(a), (b) and (c) show this fact for ε=1E-3, 1E-4 and 1E-5. The same relative error appears for $N_X = 64$, as shown in Figure 20.

6.5 Polarization and third harmonic

As in the one dimensional case, the relative error between the polarization of the exact solution and the leading term of the expansion is of order ε. Figures 21 (a) and

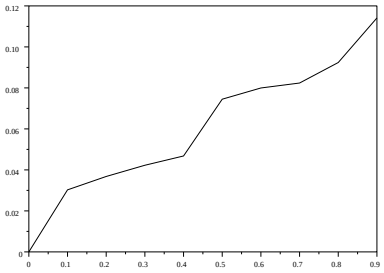

(a) $\Delta\tau$ = 1E-1

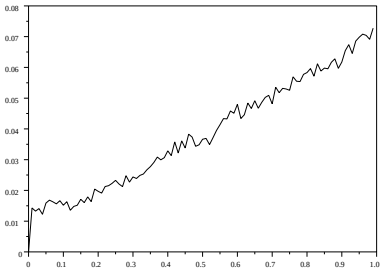

(b) $\Delta\tau$ = 1E-2

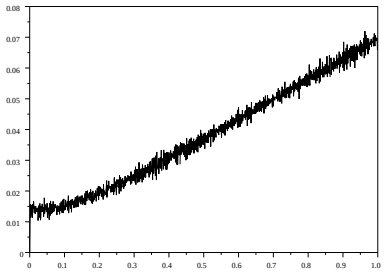

(c) $\Delta\tau$ = 1E-3

Figure 17: Relative error with respect to time in L^∞ norm between the real part of the first harmonic of the electric field given by the Maxwell-Bloch system and the solution to the NLS equation. Numerical convergence in terms of the time step. $N_X = N_Y = 128$, with ε = 1E-2

(b) confirm this fact for $N_X = N_Y$=128 and $\Delta\tau = \varepsilon$ = 1E-3 and 1E-4. The scheme preserves this precision if we decrease the number of points to 64 (see Figures 22 (a) and (b)). The third harmonic has also a preserved order of magnitude of ε^2. The Figures 23(a) and (b) show this fact for $N_X = N_Y$=128 and $\Delta\tau = \varepsilon$ = 1E-3 and 1E-4. Decreasing the number of points does not decrease the precision of the scheme, as shown in Figures 24(a) and (b).

7 Limit cases

In some cases, one suspects that the WKB expansion is not valid anymore. This occurs if ε is too large or if the H^1 norm of the initial datum is too large. Indeed, the error between the exact solution and the leading term of the profile is governed by a constant which depends on the norm of the initial data. This could arise for example in 2 cases:

- when the initial datum is stiff (that is if the amplitude is of order 1 but the

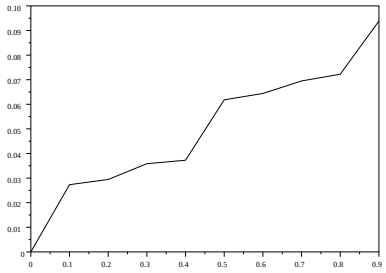

(a) $\Delta\tau$ = 1E-1

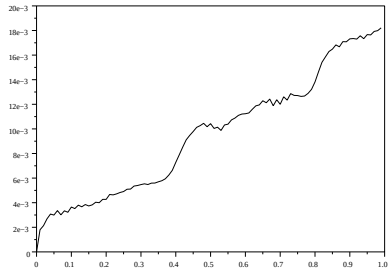

(b) $\Delta\tau$ = 1E-2

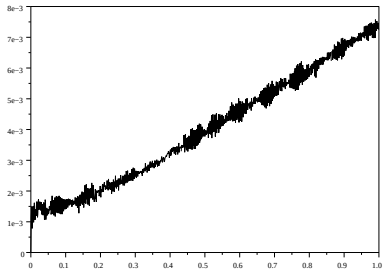

(c) $\Delta\tau$ = 1E-3

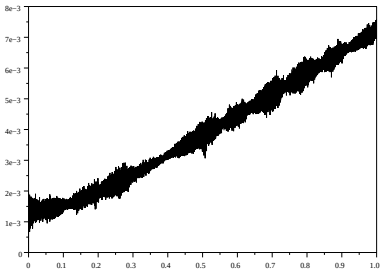

(d) $\Delta\tau$ = 1E-5

Figure 18: Relative error with respect to time in L^∞ norm between the real part of the first harmonic of the electric field given by the Maxwell-Bloch system and the solution to the NLS equation. Numerical convergence in terms of the time step. $N_X = N_Y = 128$, with ε = 1E-3

L^2-norm of the gradient is large,

- when the initial datum has a large amplitude.

Large ε When ε is large, even if N_X is large and Δt is small, the solution of the Maxwell-Bloch equations is not well approximated by the solution of NLS, and the relative error of the real part of the electric field does not match the solution of NLS. Indeed, the evolution of this relative error is of order 1E-1 (see Figure 25(a)). Figures 25 (b) and (c) represent respectively the evolution of the real part of the first harmonic of the electric field given by the Maxwell-Bloch system and the evolution of the solution to the NLS equation, with $N_X = 128$, $\Delta\tau$ =1E-3 and ε =1E-1. Figures 26 and 27 show respectively the solution of the Maxwell-Bloch equation and the one of the NLS equation, at $\tau = 0.5$, in the case $\varepsilon = 0.1$. We see the differences between these two solutions. The maximum and minimum of the Maxwell-Bloch solution is higher than those of the NLS solution. Also differences of gradient appear in the middle of the figures and in the corners.

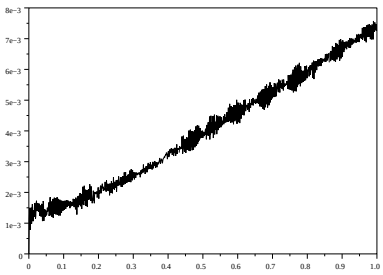

(a) $\Delta\tau = \varepsilon =$ 1E-3

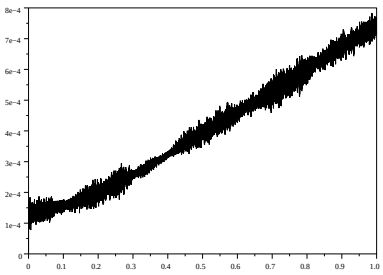

(b) $\Delta\tau = \varepsilon =$ 1E-4

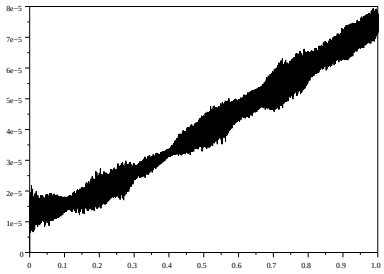

(c) $\Delta\tau = \varepsilon =$ 1E-5

Figure 19: Relative error with respect to time in L^∞ norm between the real part of the first harmonic of the electric field given by the Maxwell-Bloch system and the solution to the NLS equation. Convergence for several values of ε. $N_X = 128$ and $\Delta\tau = \varepsilon$

Stiff initial datum As initial data, we choose

$$\begin{aligned} \mathcal{W}_1^0(0,X,Y) &= e^{-92\left(X^2+Y^2\right)} \text{ for } (X,Y) \in [0,1]^2 \\ \mathcal{W}_3^0(0,X,Y) &= 0, \end{aligned}$$

that is, an initial datum which is thiner than the one used in Section 6. Figure 28 shows the relative error of the real part of the first harmonic of the electric field given by the Maxwell-Bloch system and the solution to the NLS equation. We note that the relative error is of order 20ε at $\tau = 1$, whereas it was only of order ε with the initial datum taken in Section 6 (see Figure 19).

Initial datum with large amplitude We choose an initial datum with a larger amplitude than the one used in Section 6:

$$\begin{aligned} \mathcal{W}_1^0(0,X,Y) &= 5e^{-92\left(X^2+Y^2\right)} \text{ for } (X,Y) \in [0,1] \\ \mathcal{W}_3^0(0,X,Y) &= 0. \end{aligned}$$

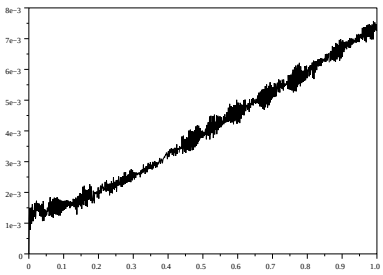

(a) $\Delta\tau = \varepsilon =$ 1E-3

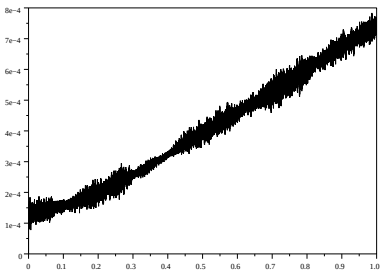

(b) $\Delta\tau = \varepsilon =$ 1E-4

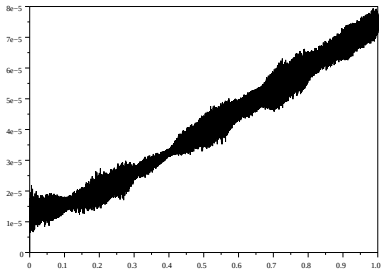

(c) $\Delta\tau = \varepsilon =$ 1E-5

Figure 20: Relative error with respect to time in L^∞ norm between the real part of the first harmonic of the electric field given by the Maxwell-Bloch system and the solution to the NLS equation. Convergence for several values of ε. $N_X = 64$ and $\Delta\tau = \varepsilon$

We note again a relative error of the real part of the first harmonic of the electric field given by the Maxwell-Bloch system and the solution to the NLS equation which is of order 60ε at $\tau = 1$, as shown in Figure 29. In addition, we also note that this relative error increases more when the H^1 norm of the Maxwell-Bloch solution is large. Indeed, figure 29 shows the evolution of the third component of the Maxwell-Bloch equations. At $\tau = 0$, $\tau = 0.41$ and $\tau = 0.82$, when the electric field is maximum, the relative error increases much more (*cf* figure 30).

These results show that the use of the nonlinear Schrödinger equation as an approximation of the electric field of the Maxwell-Bloch equation could be non well adapted. Hence the computation of the solutions of the Maxwell-Bloch equations is a necessary task.

8 Conclusion

In this paper, we have presented a Maxwell-Bloch system which modelizes the nonlinear interaction between a laser and a nonlinear medium. A numerical scheme

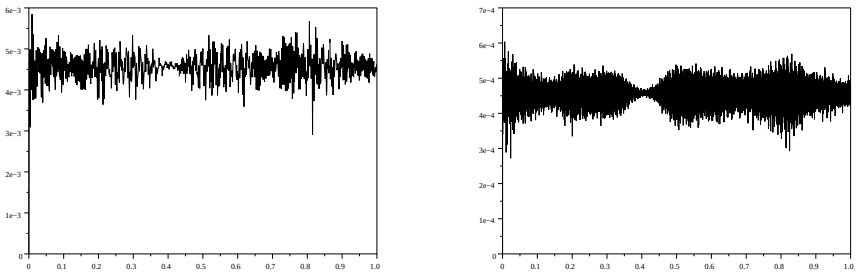

(a) $\Delta\tau = \varepsilon =$ 1E-3 (b) $\Delta\tau = \varepsilon =$ 1E-4

Figure 21: Relative error between the polarized solution and the solution (*i.e.* $\frac{|(\mathrm{I_d} - \Pi(k))E_1|_\infty}{|E_1|_\infty}$) with respect to $\tau \in [0, 1]$), with $N_X = 128$

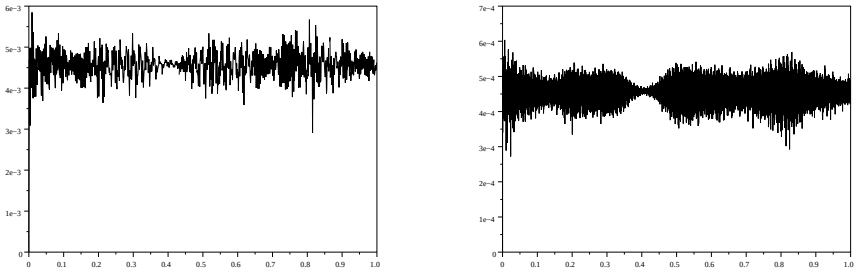

(a) $\Delta\tau = \varepsilon =$ 1E-3 (b) $\Delta\tau = \varepsilon =$ 1E-4

Figure 22: Relative error between the polarized solution and the solution (*i.e.* $\frac{|(\mathrm{I_d} - \Pi(k))E_1|_\infty}{|E_1|_\infty}$) with respect to $\tau \in [0, 1]$), with $N_X = 64$

which solves this system has been developed by using some recent results of geometrical optics. This method allows us to decouple the fast oscillating part of the solution from its envelop which varies slowly. Thus, the number of points used in the mesh decreased in an important manner (the cube of the difference of scale between the oscillations and the velocity of the envelop) compared to a usual finite difference method like the Yee scheme. In addition, the relative error between the solution of the Maxwell-Bloch equation and the one of the nonlinear Schrödinger equation (usually used when one make the paraxial approximation) is consistent with what is obtained theoretically.

Nevertheless, in some nonlinear regime, the error mentioned above is larger than the expected one and the approximation of the Maxwell-Bloch equation by the nonlinear Schrödinger equation is not valid anymore. This phenomenon occurs when the order of magnitude of the scales are not so different (large ε), or when the initial

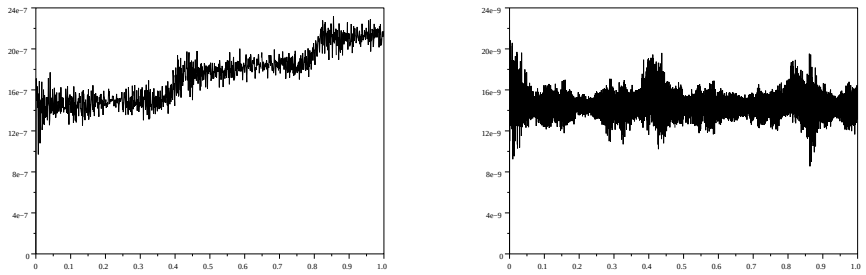

(a) $\Delta\tau = \varepsilon =$ 1E-3 (b) $\Delta\tau = \varepsilon =$ 1E-4

Figure 23: L^∞ norm of the third harmonic of the solution to the Maxwell-Bloch system with respect to time, with $N_X = 128$

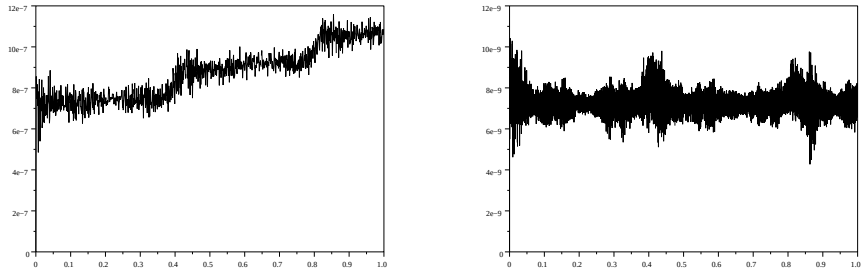

(a) $\Delta\tau = \varepsilon =$ 1E-3 (b) $\Delta\tau = \varepsilon =$ 1E-4

Figure 24: L^∞ norm of the third harmonic of the solution to the Maxwell-Bloch system with respect to time, with $N_X = 64$

data has a too large amplitude (or more generally, when its H^1 norm is large). This fact shows the importance of the computation of the solution of the Maxwell-Bloch equation in its globality.

Acknowlegment: This work has been partially supported by the ACI Jeunes Chercheurs, Ministère de la Recherche, France and GDR CNRS 2103 EAPQ.

References

[1] Alain Aspect, Claude Fabre and Gilbert Grynerg. *Introduction aux lasers et à l'optique quantique*. Ellipse - École Polytechnique, Paris, 1997.

[2] Christophe Besse, Brigitte Bidégaray and Stéphane Descombes. Order estimates in time of splitting methods for the nonlinear Schrödinger equation. *SIAM J.*

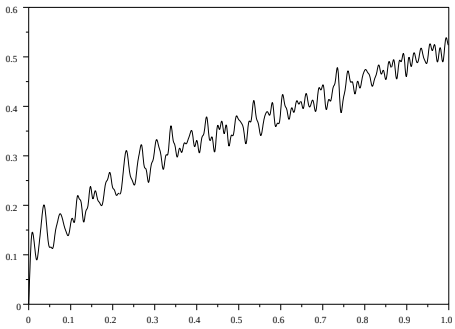

(a) Relative error with respect to time in L^∞ norm between the real part of the first harmonic of the electric field given by the Maxwell-Bloch system and the solution to the NLS equation

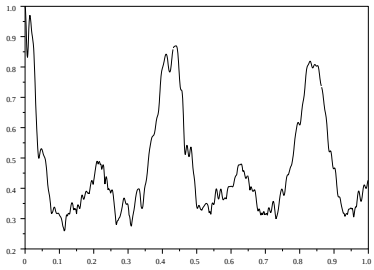

(b) Evolution of the L^∞-norm of the real part of the first harmonic of the electric field given by the Maxwell-Bloch system

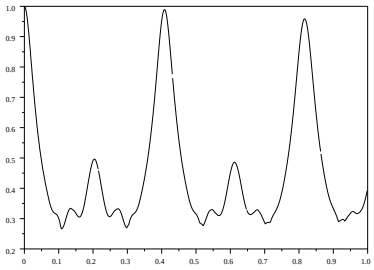

(c) Evolution of the L^∞-norm of the solution to the NLS equation

Figure 25: $N_X = N_Y = 128$, with ε = 1E-1 and $\Delta\tau$=1E-3

Numer. Anal., 40(1):26-40 (electronic), 2002.

[3] B. Bidégaray. Time discretizations for Maxwell-Bloch equations. *Methods Partial Differential Equations*, 19(3): 284-300, 2003.

[4] Robert W. Boyd. *Nonlinear Optics*. Academic Press, Inc., San Diego, 1992.

[5] T. Colin, Rigorous derivation of the nonlinear Schrödinger equation and Davey-Stewartson systems from quadratic hyperbolic systems, *Asymptotic Analysis*, 31(1):69-91, 2002.

[6] T. Colin and B. Nkonga. A numerical model for light interaction with a two-level atom medium. *Phys. D*, 188(1-2):92-118, 2004.

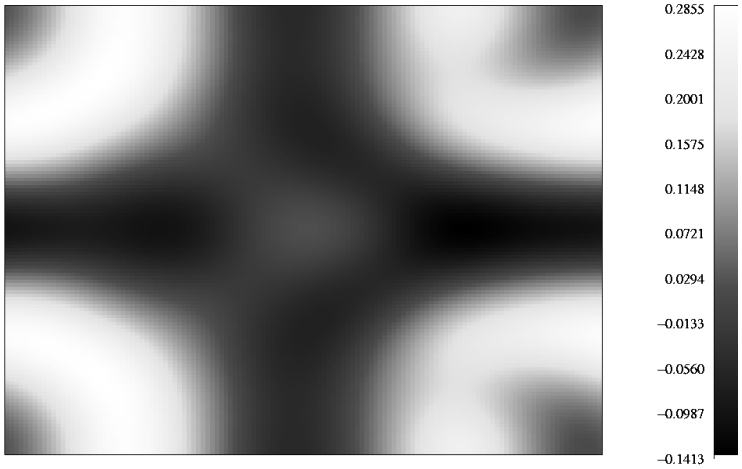

Figure 26: Real part of the first harmonic of the electric field given by the 2D Maxwell-Bloch system at $\tau = 0.5$, $N_X = N_Y = 128$, with $\varepsilon =$ 1E-1 and $\Delta\tau$=1E-3

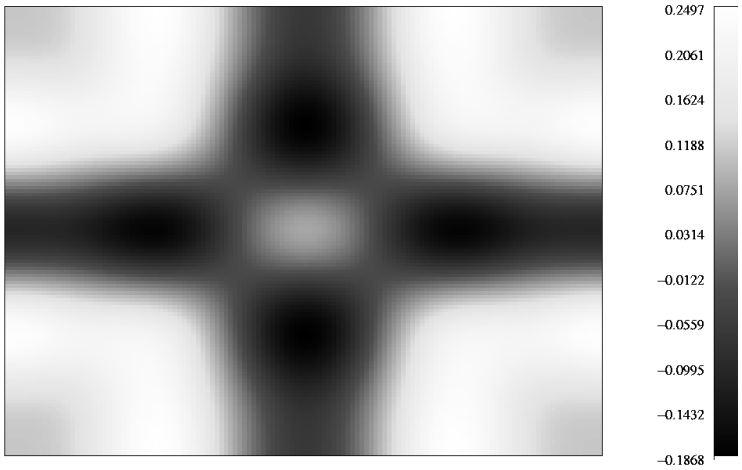

Figure 27: Solution to the NLS equation at $\tau = 0.5$, $N_X = N_Y = 128$, with $\varepsilon =$ 1E-1 and $\Delta\tau$=1E-3

[7] Claude Cohen-Tannoudji, Bernard Diu and Franck Laloë. *Mécanique quantique. Vol. I* Number 16 in Collection enseignement des sciences. Hermann, éditeur

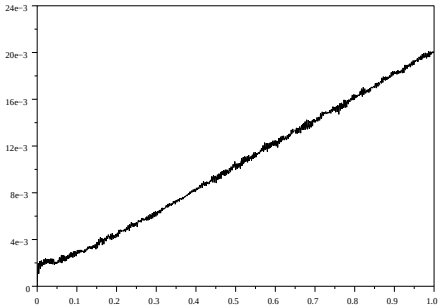

Figure 28: Relative error with respect to time in L^∞ norm between the real part of the first harmonic of the electric field given by the Maxwell-Bloch system and the solution to the NLS equation. $N_X = 128$ and $\varepsilon = \Delta\tau$=1E-3

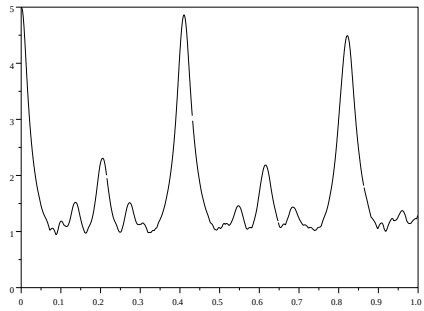

Figure 29: Evolution of the L^∞ norm of the real part of the first harmonic of the electric field e solution to the 2D Maxwell-Bloch system (26), with respect to time. $N_X = 128$ and $\varepsilon = \Delta\tau$=1E-3

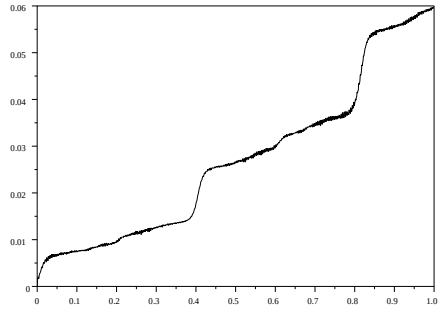

Figure 30: Relative error with respect to time in L^∞ norm between the real part of the first harmonic of the electric field given by the Maxwell-Bloch system and the solution to the NLS equation. $N_X = 128$ and $\varepsilon = \Delta\tau$=1E-3

des sciences et des arts, Paris, revue, corrigée, et augmentée d'une bibliographie étendue édition, 1973.

[8] P. Donnat, J.L. Joly, G. Métivier and J. Rauch. Diffractive nonlinear geometric optics. In *Séminaire sur les Équations aux Dérivées partielles, 1995-1996*, Sémin. Équ. Dériv. Partielles, pages Exp. No. XVII, 25. École Polytech., Palaiseau, 1996.

[9] P. Donnat. *Quelques contributions mathématiques en optique non-linéaire.* PhD thesis, Ecole Polytechnique, 1994.

[10] Philippe Donnat and Jeffrey Rauch. Dispersive nonlinear geometric optics. *J. Math. Phys.*, 38(3):1484-1523, 1997.

[11] J.-L. Joly, G. Métivier and J. Rauch. Generic rigorous asymptotic expansions for weakly nonlieanr multidimensional oscillatory waves. *Duke Math. J.*, 70(2):373-404, 1993.

[12] Jean-Luc Joly, Guy Métivier and Jeffrey Rauch. Several recent results in nonlinear geometric optics. In *Partial differential equations and mathematical physics (Copenhagen, 1995; Lund 1995)*, volume 21 of *Progr. Nonlinear Differential Equations Appl.*, pages 181-206. Birkhäuser Boston, Boston, MA, 1996.

[13] Jean-Luc Joly, Guy Métivier and Jeffrey Rauch. Recent results in nonlinear geometric optics. In *Hyperbolic problems: theory, numerics, applications, Vol II (Zürich, 1998)*, volume 130 of *Internat. Ser. Numer. Math.*, pages 723-736. Birkäuser, Basel, 1999.

[14] D. Lannes. *Quelques phénomènes d'interaction d'ondes en optique non linéaire.* PhD thesis, Université de Bordeaux I, 1999.

[15] Jerome V. Moloney nd Alan C. Newell. Nonlinear optics. *Phys. D*, 44(1-2):1-37, 1990.

[16] Olivier Saut. Computational modeling of ultrashort powerful laser pulses in a anisotropic crystal. *J. Comput. Phys. Ann*, 197(2):624-646, 2004.

[17] Bruno Sportisse. An analysis of operator splitting techniques in the stiff case. *J. Comput. Phys.*, 161(1):140-168, 2000.

[18] Gilbert Strang. On the construction and comparison of difference schemes. *SIAM J. Numer. Anal.*, 5:506-517, 1968.